Journal of Pharmaceutical Analysis 13 (2023) 694–710

Contents lists available at ScienceDirect

Journal of Pharmaceutical Analysis

journal homepage: www.elsevier.com/locate/jpa

Review paper

Dissecting the brain with spatially resolved multi-omics

Yijia Fangma [a,1], Mengting Liu [a,1], Jie Liao [b,1], Zhong Chen [a,*], Yanrong Zheng [a,**]

[a] Key Laboratory of Neuropharmacology and Translational Medicine of Zhejiang Province, School of Pharmaceutical Sciences, Zhejiang Chinese Medical University, Hangzhou, 310053, China
[b] Pharmaceutical Informatics Institute, College of Pharmaceutical Sciences, Zhejiang University, Hangzhou, 310058, China

ARTICLE INFO

Article history:
Received 31 October 2022
Received in revised form
4 April 2023
Accepted 6 April 2023
Available online 10 April 2023

Keywords:
Central nervous system disorders
Multi-omics
Spatial transcriptomics
Spatial proteomics
Spatial metabolomics

ABSTRACT

Recent studies have highlighted spatially resolved multi-omics technologies, including spatial genomics, transcriptomics, proteomics, and metabolomics, as powerful tools to decipher the spatial heterogeneity of the brain. Here, we focus on two major approaches in spatial transcriptomics (next-generation sequencing-based technologies and image-based technologies), and mass spectrometry imaging technologies used in spatial proteomics and spatial metabolomics. Furthermore, we discuss their applications in neuroscience, including building the brain atlas, uncovering gene expression patterns of neurons for special behaviors, deciphering the molecular basis of neuronal communication, and providing a more comprehensive explanation of the molecular mechanisms underlying central nervous system disorders. However, further efforts are still needed toward the integrative application of multi-omics technologies, including the real-time spatial multi-omics analysis in living cells, the detailed gene profile in a whole-brain view, and the combination of functional verification.

1. Introduction

Mammalian brains are unique in their heterogeneity and are characterized by complex functional division and dramatic diversity among cell-types [1,2]. Neuronal cells in different brain regions constitute a three-dimensional (3D) communication network, laying the foundation for the functional diversity of the brain [3]. Abnormal organization of the brain spatial network leads to a number of central nervous system (CNS) disorders like neuropsychiatric [4] and neurodegenerative disorders [5], which collectively constitute a major global health problem due to growing prevalence and generally poor outcomes [6]. Undoubtedly, the remarkable spatial heterogeneity of the brain makes it difficult to identify drug targets for CNS disorders. At the same time, the spatial heterogeneity of the human brain provides opportunities to develop precise targeted therapies once detailed biomolecule expression profiles and corresponding functional annotations are fully understood [7–10].

Spatial multi-omics is a novel approach to reveal the complex structural, neurochemical, genetic, and functional heterogeneity of the human brain. By separating different areas of the brain and marking spatial information, spatial omics can collect valuable information on tissues [11,12]. Depending on research objectives, spatial-omics can be divided into spatial genomics, spatial transcriptomics, spatial proteomics, and spatial metabolomics. Spatial transcriptomics is the most well-established spatial-omics technology for analyzing the spatial heterogeneity of gene expression levels in tissues [13–17] and has been voted as one of the seven technologies to watch in 2022 by Nature [18]. Thanks to the development of single cell sequencing, spatial transcriptomics can also be used to find key genes in the processes of tissue development, functional zoning, disease development, etc. at the single cell level. Yet in human cells, the protein concentrations are only weakly correlated with messenger RNA (mRNA) abundance due to multiple protein regulatory pathways including protein degradation [19]. After translation, proteins undergo complex processing (e.g., folding [20] and modifications [21]) that is critical for functional regulation [22], but this post-translational processing cannot be detected by transcriptomics alone. In contrast, newly developed spatial proteomics can detect these modifications. Lipids are also essential components of cells, exhibiting key functions in metabolism and membrane structure, and provide a direct cellular metabolic status [23]. In addition, the metabolism of nerve cells is vigorous, and the types and levels of small molecule metabolites in neuronal cells are closely related to the regulation

Peer review under responsibility of Xi'an Jiaotong University.
* Corresponding author.
** Corresponding author.
E-mail addresses: chenzhong@zju.edu.cn (Z. Chen), yanrong_zh@zju.edu.cn (Y. Zheng).
[1] These authors contributed equally to this work.

https://doi.org/10.1016/j.jpha.2023.04.003

of neuronal function [24,25]. Spatial metabolomics is a new strategy to study the spatial heterogeneity of lipids and small molecule metabolites.

At present, comprehensive analysis from mRNA to proteins and metabolites is a general trend, and integration of studies with spatial-omics is highly recommended due to the fact that the level of mRNA sometimes does not accurately reflect the expression abundance of the corresponding protein [26,27]. Furthermore, computational integration of multi-omics data has a higher sensitivity in discovery of specific contributors. For example, the integrated parallel single-cell DNA and RNA analysis found that major histocompatibility complex class-I downregulation is a specifically dysregulated in triple-negative breast cancer, but it's not be seen in either sequencing method alone [28]. On the other hand, specific substances or pathways found by each omics data can be evidence of each other. A comprehensive multi-omics analysis like proteomics, RNA sequencing and chromatin immunoprecipitation sequencing of Alzheimer's disease (AD) brains co-support the upregulation of histone H3 acetylated lysine 27 (H3K27ac) and histone H3 acetylated lysine 9 (H3K9ac), which were linked to transcription, chromatin, and disease pathways in AD [26]. Therefore, the integration of multi-omics data shows the great potential ability to synthesize more information from a ton of datasets than individual measurements. Here, we review the basic principles of various spatial omics techniques as well as the computational approaches for spatial omics. Furthermore, we discuss the applications of spatially-resolved multi-omics in the CNS, highlighting their contributions to revealing spatial heterogeneity of the brain and deciphering pathological mechanisms underlying CNS disorders. More detailed information on these technologies and applications in neuroscience is present in the Supplementary data, including the "Spatial transcriptomics" and "Spatial metabolomics and proteomics" sheets.

2. Development of spatial transcriptomic technologies

Spatial transcriptomics technologies are categorized into two major approaches: next-generation sequencing (NGS)-based technologies, which assess the location of transcripts before NGS sequencing, and image-based technologies including in situ hybridization (ISH) and in situ sequencing (ISS) methods.

2.1. NGS-based spatial transcriptomics technologies

NGS-based spatial transcriptomics technologies can be further divided into three categories based on the ways retaining spatial information before RNA sequencing. The first approach is characterized by physical dissection with subsequent spatial information labeling, among which laser capture microanatomy (LCM)-based technologies are most well-established (Fig. 1). For LCM, the tissues are sectioned into slices which are stained and imaged under a microscope. Subsequently, the targeted regions are cut off using a microscope-guided laser and captured in pre-labeled containers to maintain spatial information. The tissues captured in different containers are further subjected to RNA extraction and reverse transcription. During RNA reverse transcription, a unique known sequence (termed barcode) will be added in each container and subsequently introduced to the complementary DNA (cDNA), after which samples from different containers can be pooled for RNA sequencing [29,30]. Theoretically, LCM can also be applied to harvest single cells. However, the collection of enough single cells for building a spatial map is labor-consuming, and the efficiency of a single cell accurately falling into a given container is relatively low. To cope with these issues, Jing and co-workers [31,32] proposed an LCM-based and single-cell-seq-data-corrected spatial transcriptomics technology, called geographical position sequencing (Geo-seq). In Geo-seq, LCM is employed first to establish a spatial map landmarked with various spatially enriched genes (named zip-code genes) and then the single cells will be localized to this map according to single-cell RNA-seq data and zip-code. Based on LCM, Geo-seq can be less restricted by the amount of sequencing materials, but laborious since highly resolved zip-code genes are obtained by manually isolating single cells. In addition, traditional LCM-based spatial transcriptomics technologies are usually applied to capture discrete sporadic samples, resulting in a fragmented and incomplete transcriptome map. Another microdissection-based technology, Tomo-seq first proposed by Junker et al. [33], solved this problem by consecutively cryosectioning individual pallets of tissue in three orthogonal directions (*X*, *Y*, and *Z* axes). RNA extracted from every section will further go through barcode incorporation during reverse transcription to retain the spatial information. The RNA expression profiles along the three axes are further mathematically reconstructed to build a 3D expression atlas [33]. During the mathematical reconstruction, the reads of a given gene are first distributed along the *X* axis leaving the reads distributed evenly in the other two directions. Then, the sequencing reads are redistributed along *Y* axis with the *X* position of each read unchanged. Similarly, the reads undergo the third distribution along the *Z* axis. Finally, with iterative proportional fitting algorithm, the RNA expression pattern is mapped to a 3D binary tissue image initially captured by a selective plane illumination microscopy [33]. To further reach the single-cell resolution, Lee et al. [34] developed XYZeq, which maintains both spatial information and single-cell identity via two rounds of polymerase chain reaction (PCR) indexing. Briefly, the tissue cyro-section is partitioned by a microwell array, each well of which provides unique primers along with

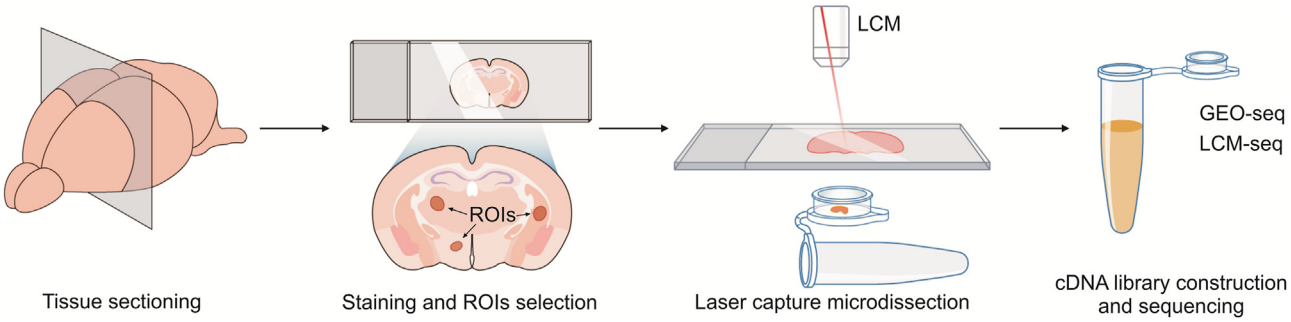

Fig. 1. The diagram of laser capture microanatomy (LCM)-based spatial transcriptomics technologies. Tissues are sectioned, stained and imaged for morphology. Subsequently, the regions of interest in the tissue are cut off using a microscope-guided laser and captured in different containers for sequencing. ROI: region of interest; Geo-seq: geographical position sequencing; cDNA: complementary DNA.

cell dissociation/permeabilization buffer to label spatial positions via intracellular reverse transcription. Next, the intact cells are selected, pooled, and finally split into other plates in a one-cell-one-well manner, and each well of the new plates contains barcoded primers to mark the single-cell identity. After combinatorically barcoding, all cDNAs finally are mixed for sequencing.

In addition to barcoding after physical dissection, biomolecules can also be in situ barcoded in a nondestructive way (Fig. 2). Briefly, barcodes can be introduced to the targeted proteins through antibody, and targeted RNA through hybridization. The barcodes will then be retrieved from tissue and go through NGS to analyze the expression profiles of targeted biomolecules. Typically, in digital spatial profiling (DSP) technology, the photocleavable oligonucleotide barcodes (PC-oligos) are employed and covalently attached to mRNA probes or protein antibodies (Fig. 2A) [35,36]. After being incubated with these PC-oligos-tagged probes or antibodies, the ultraviolet (UV) light illuminates a selected area (covering 1 to ~5000 cells) of the tissue to release the PC-oligos which are subsequently collected by microcapillary aspiration. Another tool, deterministic barcoding in tissue for spatial omics sequencing (DBiT-seq) has ability to label spatial information through a pair of microfluidic chips (Fig. 2B) [37]. Each microfluidic chip contains 50 parallel microchannels (down to 10 μm in width). One microfluidic chip is employed first to introduce barcodes (X_1–X_{50}) in one direction (X) and the barcodes bind to the polyA-tail of mRNA via their poly(d)T sequence. After removing the first microfluidic chip, the second microfluidic chip is attached to the tissue to introduce another set of barcodes (Y_1–Y_{50}) in the orthogonal direction (Y). In this way, the RNA expression profile of a given area can be reconstructed with its spatial barcode (X_iY_j, $i = 1$–50, $j = 1$–50). To simultaneous detection of proteins and mRNA, antibodies tagged with indexed DNA sequences are incubated with tissue at the beginning. Those indexed DNA tags also embrace poly(d)A segment in their sequences, which is critical to subsequent spatial barcodes binding. Despite the failure in proteome-wide detection, DSP and DBiT-seq still provide practical tools for the integration of spatially resolved multi-omics.

The third way to retain spatial information for NGS is to capture biomolecules in a solid surface bearing an oligonucleotide barcode array (Fig. 3) [38]. Generally, each oligonucleotide barcode contains a PCR handle (for linear amplification of cDNA library), a spatial barcode (for labeling spatial positions), a unique molecular identifier (for distinguishing intracellular mRNA copies from their PCR amplification products), a poly(d)T region (for mRNA capture), and a cleavage sequence (for solid surface attachment and dissociation) [38]. Typically, in spatial transcriptomics (ST) technology, ~200 million capture oligonucleotides in each of 1007 spots (100 μm in diameter, 200 μm in center-to-center distance) are arrayed over an area of 6.2 mm by 6.6 mm [38]. Since the spatial barcode region of the oligonucleotides in each spot share the identical sequence, the center-to-center distance represents the spatial resolution. Visium, proposed by 10x Genomics, has reached higher spatial resolution by spreading capture oligonucleotides in ~5000 spots (55 μm in diameter, 100 μm in center-to-center distance) spanning 6.5 mm × 6.5 mm area [15,39,40]. In addition to be ligated directly to a solid surface, capture oligonucleotides can also attach indirectly via microparticles. Rodriques et al. [41] developed a beads-based spatial transcriptome technology called Slide-seq. These beads are 10 μm in diameter and each bead distinct capture oligonucleotides. After being deposited in a one-beside-another manner, the beads form a monolayer over a rubber-coated glass coverslip and are then spatially indexed by oligonucleotide ligation and detection (SOLiD) sequencing. By employed barcoded beads, Slide-seq has almost reached a single-cell resolution (10 μm). Similarly, Vickovic et al. [42] developed high-definition spatial transcriptomics (HDST) by randomly spreading capture oligonucleotides-bearing beads into the 2 μm wells of a hexagonal array. The spatial barcode of distinct well will then be determined by sequential hybridization [42]. The methods mentioned above directly load sectioned tissue onto a pre-barcoded solid surface while some approaches are performed in a different way by extracting and transferring RNA transcripts from pre-attached tissue slices to another barcoded solid surface. For example, another technology, sci-Space, incubates tissue slices with spatial barcodes (termed as hashing oligos) which subsequently permeate into and

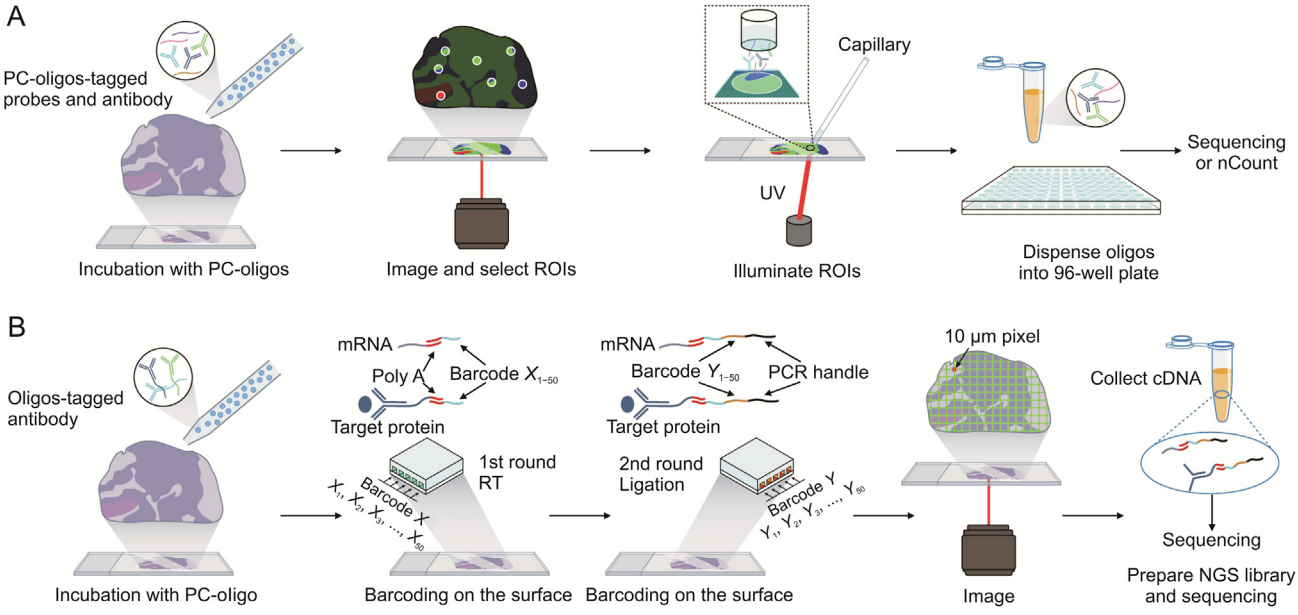

Fig. 2. The diagram of next-generation sequencing (NGS)-based technology: (A) digital spatial profiling (DSP) and (B) deterministic barcoding in tissue for spatial omics sequencing (DBiT-seq). PC-oligos: photocleavable oligonucleotide barcodes; ROI: region of interest; UV: ultraviolet; mRNA: messenger RNA; Poly A: polyadenylate tails at the 3' end of messenger RNAs; RT: reverse transcription; PCR: polymerase chain reaction; cDNA: complementary DNA.

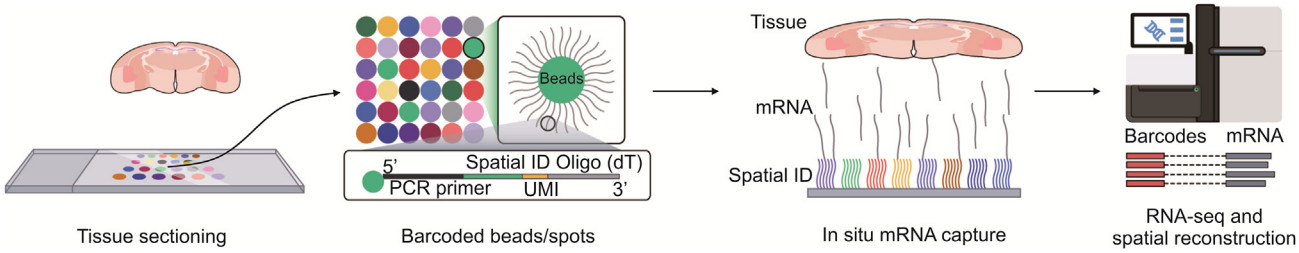

Fig. 3. The diagram of spatial transcriptomics (ST) technology. Tissue is sectioned and attached to a glass slide bearing a set of barcoded DNA oligonucleotide capture probes. RNA sequencing (RNA-seq) is performed after in situ messenger RNA (mRNA) capture. The spatial transcriptomic profile will be reconstruction according to spatial barcodes. PCR: polymerase chain reaction; UMI: unique molecular identifier.

label the nuclei [43]. These hashing oligos spots (~146.4 μm in diameter, 222 μm in center-to-center distance) are arrayed in grid (18 mm^2 area) on a glass slide [44]. The hashing oligos are transferred to tissue by juxtaposing two slides face-to-face, after which labeled nuclei will be isolated and pooled for combinatorial barcoding (similar to XYZeq) to retain single-cell identity. Obviously, sci-Space achieves the spatial transcriptomic analysis for wide anatomical regions and retains the single-cell resolution. However, sci-Space is still limited by low spatial resolution (>200 μm) and inefficient cell recovery. Recently, Chen et al. [45] proposed another spatial transcriptome technology in large-field of view, called spatial enhanced resolution omics-sequencing (Stereo-seq). Stereo-seq is developed from the DNA nanoball (DNB) sequencing technology in which chips etched with DNBs are employed to capture mRNA [46]. In Stereo-seq, each chip harbors 400 DNBs (220 nm in diameter, 500 nm in center-to-center distance) over a 100 μm^2 area and further joints together with each other to cover an mRNA-capturing area of up to 13.2 cm^2 [45]. Each DNB in the chip contains distinct barcodes which can be spatially indexed by DNB-based in situ sequencing [45,46]. In this way, Stereo-seq can profile the gene expression of large-size tissue at a near-subcellular resolution.

2.2. Image-based technologies

Although NGS-based spatial transcriptomic technologies have high throughput and good depth, they cannot achieve in situ transcriptome detection. In contrast, image-based technologies aid in in situ transcriptome detection and capture the transcriptome at higher spatial resolution than NGS-based technologies, even reaching the subcellular level. Image-based technologies can be divided into two major types: ISH- and ISS-based spatial transcriptome methods (Fig. 4).

Fluorophore-labeled RNA or DNA complementary hybridization probes are the basis for ISH. Early technology called single-molecule fluorescence in situ hybridization (smFISH) detects the fluorescence of these probes after their hybridization with specific mRNA to realize the visualization of the corresponding mRNAs in a subcellular resolution [47]. Obviously, smFISH can only deal with limited numbers of targets. To improve the sequencing depth and coverage, ISH technologies are challenged by high background and low resolution caused by molecular stacking. To overcome these shortcomings, next-generation ISH technologies have been developed using sequential rounds of hybridization and imaging of fluorophore-labeled oligonucleotides. Multiplexed error-robust FISH (MERFISH) technology, developed by Zhuang and co-workers [48], is based on a set of well-designed encoding probes, which contains targeting sequences for RNA binding and readout sequences for barcoding (Fig. 4A) [48]. The readout sequences for corresponding targeting sequences are pre-indexed and therefore each RNA species can be translated to a unique combination of readout sequences. After the hybridization of encoding probes, fluorophore-labeled readout probes, which specifically bind the readout sequences in encoding probes, are added and imaged for successive rounds. The fluorophore detected is photobleached between readout probe hybridization rounds. In each round, readout probes with distinct sequences are employed and the fluorescence of each RNA species is encoded binarily (1 for fluorescence detected after a successful hybridization event and 0 for no fluorescence detected). The binary codes of RNA species will be decoded with complex algorithm [48–50]. Theoretically, with 16 rounds of readout hybridization, over 64,000 (2^n–1) RNA species can be identified [48]. However, increased rounds of readout hybridization dramatically decrease the number of successful hybridization events, resulting in up to 1001 RNA species detected by the very first version of MERFISH [48]. With optimized error-correcting encoding scheme, updated decoding algorithm, and the application of expansion microscopy, MERFISH has almost enabled a genome-wide spatial transcriptome [51,52]. More importantly, MERFISH can position a single RNA molecule within the cell by simultaneously visualizing cellular compartments (like endoplasmic reticulum and nucleus) with immunofluorescence. Unlike MERFISH using only one type of fluorophore, sequential fluorescence in situ hybridization (seqFISH) increases the number of fluorophores to 4 types thus reducing the cycles of hybridization to 8 (4^8 > 64,000) [53] (Fig. 4A). However, the diversity of fluorophores along with molecular stacking cause remarkable optical crowding and make it difficult to image clearly. Thus, Lubeck and Cai [54] combined super-resolution microscopy with seqFISH for a higher resolution. However, super-resolution microscopy takes longer time in imaging and is limited by higher technique requirements and narrow scope of application in thin samples. To further overcome these limitations, Cai and co-workers [55] has proposed seqFISH$^+$ by using 60 pseudocolor channels instead of 4–5 fluorophores. These pseudocolours are assigned into three fluorescent channels (Alexa Fluor 488, Cy3b, and Alexa Fluor 647; 20 pseudocolors per channel), which can be detected by conventional confocal microscopy. Therefore, three rounds of readout hybridization are enough for a near-genome-wide transcriptomic analysis ($3 \times 20^3 = 24{,}000$). In practice, seqFISH$^+$ is performed with four rounds of readout hybridization including one round of error correction [55]. Notably, seqFISH-based technologies can also be applied to study single-nucleotide polymorphisms [56] and chromosome loci [57]. Obviously, ISH-based methods provide powerful tools for spatial transcriptomic analysis. However, it still needs to be mentioned that these methods work robustly for known sequences and less likely identity novel transcripts or gene mutations since they are based on probe hybridization.

Another major type of image-based transcriptome technology is ISS-based technology which can be further divided into targeted and untargeted approaches. As a targeted ISS technology,

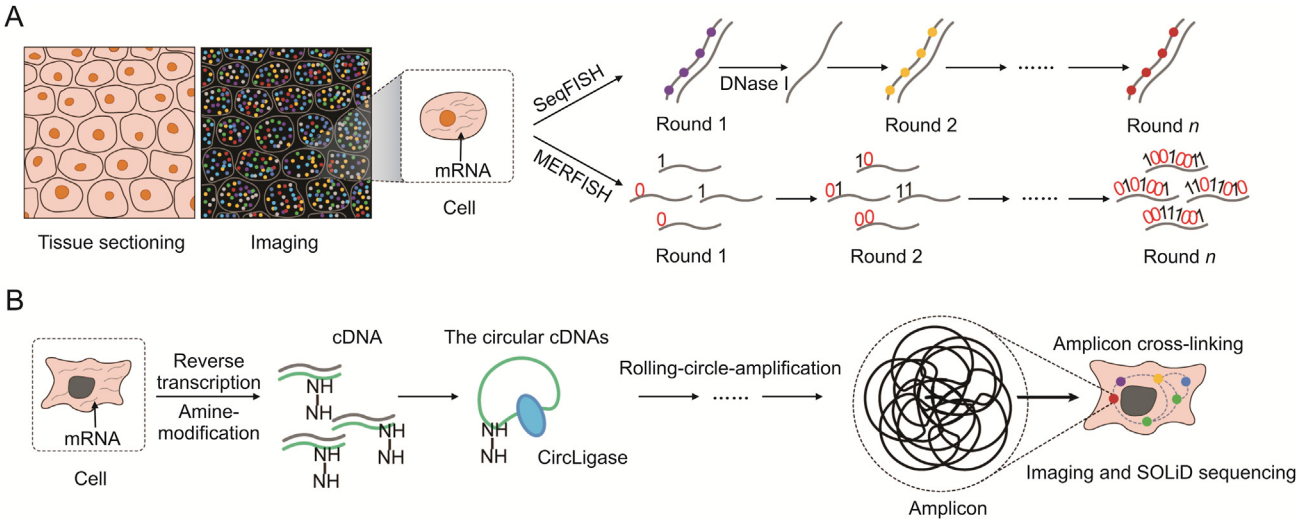

Fig. 4. The diagram of image-based technology. (A) In situ hybridization (ISH)-based method including sequential fluorescence in situ hybridization (seqFISH) and multiplexed error-robust FISH (MERFISH). (B) In situ sequencing (ISS)-based method. mRNA: messenger RNA; cDNA: complementary DNA; SOLiD: sequencing by oligonucleotide ligation and detection.

spatially-resolved transcript amplicon readout mapping (STARmap) technology actually reads out the sequence of barcodes rather than targeted transcripts by sequencing [58]. The first step of STARmap bypasses the reverse transcription and involves padlock probes-based in situ amplification of cDNA [59]. These padlock probes (termed SNAIL probes [58]) contain targeting sequence for RNA binding and targeting-sequence-coupled barcode sequence. By rolling-circle-amplification (RCA), padlock probes further generate DNA nanoballs each of which contains multiple copies of the original barcode sequence. The DNA nanoballs subsequently is transferred to gels (called DNA hydrogels), during which the 3D distribution pattern of DNA nanoballs will be maintained to retain spatial information. Finally, the barcodes are read out in the hydrogels by the sequencing-by-ligation technology and the corresponding transcripts can be mapped to the tissue image [58]. Using this method, it is possible to profile ~1000 genes three-dimensionally in tissue slices by STARmap [58]. Another targeted sequencing technology, barcode in situ targeted sequencing (BaristaSeq) uses the gap padlock probe for in situ barcode sequencing, resulting in compatibility with Illumina sequencing platform and higher amplification efficiency [60]. As a well-established untargeted approach, fluorescence in situ sequencing (FISSEQ) employs CircLigase to circularize cDNA after reverse transcription. The circular cDNAs then go through RCA to amplify their original sequences and generate DNA amplicons. Importantly, PEGylated bis(sulfosuccinimidyl)suberate (BS(PEG)9)-mediated cross-linking is applied to stabilize the amplicons, after which SOLiD sequencing is performed to read out the gene profile (Fig. 4B) [61]. So far, FISSEQ fails to detect genes with low-expression due to the inefficient reverse transcription and it also works mainly in cultured cells [61]. Recently, Alon et al. [62] proposed a novel ISS approach applicable to tissue samples, called expansion sequencing (ExSeq). This method combines FISSEQ with expansion microscopy to achieve a nanoscale resolution [62]. Briefly, the RNA molecules are anchored in a gel material. The gel physically expands ~4-fold in water enabling nanoscale imaging with conventional confocal microscope. Moreover, the increased spatial distance between RNAs making RNAs more accessible, thus increasing the efficiency of reverse transcription and amplification with FISSEQ. However, FISSEQ is limited by its short reads (5–30 bp). To improve the gene coverage, the cDNA nanoballs (amplified during FISSEQ) are extracted and subjected to NGS. Brilliantly, the transcripts readout from NGS can be remapped to tissue images according to the short reads provided by FISSEQ data [62].

So far, except XYZeq, Sci-space, FISSEQ, and BaristaSeq, other spatially-resolved technologies mentioned above have already been applied in neuroscience [3,41,42,55,58,62–68]. In summary, among spatial transcriptomics technologies mentioned above, microdissection-based technologies tend to be more labor-intensive. Through the combination of unbiased cryo-sectioning and computational analysis, Tomo-seq has saved time to some extent by skipping manual tissue selection and capture. However, since the slices in three directions are from distinct samples in the Tomo-seq protocol, it may not be applicable to clinical samples which are usually unique and lack duplicates. Moreover, although LCM is capable of single-cells-isolation, the heat generated by laser during microdissection will undermine the integrity of RNA. XYZeq improves the spatial resolution of LCM to the single-cell level through chemical digestion combined with two rounds of indexing, saving time and labor to obtain single cells and improving the RNA quality. However, due to the limitation of barcode diversity and the cost of barcode synthesis, this technique is more suitable for research with definitely targeted regions of interest rather than searching for the region with the most obvious transcriptomic change in whole tissue. This limitation may be not ignored in the context of CNS disorders since these pathological states are usually the overall outcome of a dysfunctional brain network involving diverse brain regions. Although image-based technologies, including MERFISH, seqFISH, and FISSEQ, show the most impressive spatial resolution, these methods are technically difficult and highly dependent on computational analysis. Fortunately, the commercial sequencing platform based on MERFISH, MERSCOPETM, has been launched. This all-in-one platform for spatial profiling and analyzing undoubtedly makes the MERFISH protocol more automatic and repeatable. Its application in clinical samples and performance when facing large sample sizes are definitely worthy of expectation. When it comes to commercialization and popularization, ST technology and Visium are so far the most famous and easily accessible. As mentioned above, these technologies actually provide bulk transcriptomic data of extremely tiny regions instead of single cells. In addition, due to high cost, the spatial coverage of ST technology is quite limited, so this technology

is more suitable for assessing certain layers of interest in sample tissues. As the pioneer in spatially-resolved multi-omics technology, DSP provides a valuable platform for integrated analysis of spatial transcriptomic and proteomic data. Although limited by low spatial resolution, DSP greatly helps to narrow down the region of interest which could be further analyzed by single-cell RNA sequencing to obtain detailed information about cell subpopulations. Detailed comparisons of different spatially-resolved transcriptomic techniques are listed in Table S1 [30,32–34,36–38,40–42,44,45,47–50,55,58,60–62,67].

3. Spatial transcriptomics technologies in neuroscience

Spatial transcriptomics technologies have been widely used in neuroscience research in view of their current benefits. Here we discuss four fields that may particularly benefit from spatial transcriptomics technologies: building the brain atlas, uncovering gene expression patterns of neurons for special behaviors, deciphering the mechanism underlying neurological diseases, and understanding the molecular basis of neuronal communication.

3.1. Building the brain atlas

The brain is an incredible machine consisting of approximately 100 billion cells [69], therefore establishing a molecular map is a crucial step in understanding the functional diversity of brain. Here, we also describe several examples of how spatial transcriptomics technologies can be used to generate the brain molecular atlas. Ortiz et al. [63] used the ST method to build a molecular atlas of the whole brain in adult mice. Similarly, Fang et al. [50] constructed a spatial atlas of the human middle and superior temporal gyrus by MERFISH and showed that the cellular composition of these cortical regions in humans differs from that in mice. Tavares-Ferreira et al. [70] used 10× Visium to profile the spatial distribution of cell subpopulations in the dorsal root ganglia (DRG) of human. They also compared DRG neuronal populations of humans to those of nonhuman primates and identified nociceptor subtypes with special pathological significance for pain in humans [70]. The cerebellum is related to motor function, cognition, emotion regulation, and language. Using the LCM method, Aldinger et al. [71] generated gene expression profile maps of the human cerebellum during development. Moreover, by mapping the genes associated with Joubert syndrome and AD, the authors identified the key cell types in these two neurological disorders. Shah et al. [67] found that there were conflicting descriptions of hippocampal organization proposed in recent RNA-seq data and in the Allen Brain Atlas data. Therefore, they employed seqFISH to profile gene expression in the hippocampus at single-cell resolution. Their results revealed that the cell heterogeneity determined by gene expression recapitulates the anatomical subpopulations in the dentate gyrus. More importantly, they further uncover the heterogeneity of cell populations in CA1 and CA3 [67].

3.2. Uncovering gene expression pattern of neurons for special behaviors

Spatial transcriptomics have provided researchers with groundbreaking insights into the molecular basis of certain brain functions. For instance, the hypothalamus controls diverse social behaviors including mating, parenting, and aggression, yet the molecular basis of these behaviors is poorly understood. Moffitt et al. [49] combined MERFISH with single-cell RNA-seq to create a spatially resolved cell atlas of the mouse hypothalamus preoptic region, and identified about 70 different neuronal subtypes. Furthermore, by combining immunostaining for cfos (a marker for neuronal activation), MERFISH revealed the key markers of cfos-positive neurons in the brain slices of mice subjected diverse behavior tests. In this way, the gene profile of specific cell types responsible for different social behaviors can be identified [49].

3.3. Deciphering the mechanisms underlying neurological diseases

Spatial transcriptomics technology provides a new approach to study the pathological changes of diseases. Using the 10× Visium method, Maynard et al. profiled the gene expression in the human dorsolateral prefrontal cortex, a region involved in several neuropsychiatric disorders, at high spatial resolution [15]. Integrating neuropsychiatric disorder gene sets, they subsequently showed the layer-specific expression of genes relevant to schizophrenia and autism spectrum disorder. By employing single-cell RNA-seq to sort 8016 cells from six wild-type and AD model mice, Keren-Shaul et al. [65] identified a novel microglia cell type termed disease microglia (DAM). They further applied smFISH to locate the DAM and found that they were located in proximity to Aβ plaques. Intriguingly, gene set enrichment analysis suggested that DAM are highly expressing phagocytic gene. Taken together, these results imply that DAM are responsible for plaque clearance in AD [65]. Astrocytes are also known to be involved in AD pathogenesis. Hasel et al. [64] combined single-cell RNA-seq with 10× Visium to categorize and position the astrocyte subtypes in the brain exposed to different inflammatory stresses (lipopolysaccharide or interferon).

In addition, a comprehensive understanding of the transcriptome spectrum of a disease helps in identifying potential therapeutic targets. Using the ST technology, Navarro et al. [13] identified the genes that are differentially expressed in the hippocampal and olfactory bulb regions of control and AD model mice. Furthermore, the authors mined the reported data on these gene's expression in the brains of AD patients. Notably, they have found Bcl-2-related ovarian killer (BOK), a mitochondria-located protein involved in apoptosis [72] and mitochondrial dynamics [73], was downregulated in both AD model mice and AD patients. This finding supports the widely held notion that dysfunctional mitochondria contribute to AD pathology [74] and further identifies BOK may be a potential therapeutic target for AD. In another study, Chen et al. [14] first employed ST to identify the significantly altered pathways in AD mice and then confirmed the alteration at single-cell resolution. The data showed that myelination-related oligodendrocyte genes and inflammation-related plaque-induced genes play essential roles in the early and late phases of AD, respectively [14]. Maniatis et al. [75] used ST to obtain gene expression data from amyotrophic lateral sclerosis (ALS) patients and mice over the course of the disease to reveal the molecular pathological mechanism of ALS. The results showed that sphingolipid signaling pathways are shared by ALS mice and patients. Supportively, modulators of sphingolipid signaling had already been proposed as potential therapeutics for ALS [76,77]. Similarly, Gregory et al. [78] analyzed the transcriptome of brain tissues from ALS patients including chromosome 9 open reading frame 72, sporadic ALS, and superoxide dismutase 1 mutant cases using ST technology, and identified two spatially dysregulated genes, namely ubiquitin specific peptidase 47 and metabotropic glutamate receptor 3, which may be responsible for the regional vulnerability to ALS.

Spatial transcriptomic technologies supply single-cell sequencing data with spatial information to distinguish key pathological targets whereas CNS disorders tend to be the overall outcome of a dysfunctional brain network involving diverse brain regions. For example, the heterogeneity of diffuse midline glioma-H3K27 M mutant (DMG) and glioblastoma (GBM) has been established by single-cell RNA-seq [79,80]. However, the spatial distribution of different cell types in DMG and GBM remains elusive. Recently, by performing spatial profiling of DMG and GBM

combining short- and long-read spatial transcriptomics, Ren et al. [8] found that oligodendrocyte precursor-like cells mainly cluster in the tumor core while radial glial stem-like (RG-like) cells aggregate in the neuron-rich invasive niche in both cancers. These data suggest that these two cell types have different roles and RG-like cells are more relevant to tumor invasion, which cannot be elucidated without spatial information. Further combining 10× Visium technology, they functionally identified a novel target (FAM20C) for DMG which mediates the invasive growth of RG-like cells in a neuron-rich microenvironment. Similarly, Ji et al. [9] combined single-cell RNA-seq with ST technology, and found tumor-specific keratinocyte (TSK) localized to a fibrovascular niche and TSK-enriched integrin signaling genes integrin β1 and fermitin family homolog 1 inhibit the anti-tumor immune response. Furthermore, by employing light-sheet imaging, Kirschenbaum et al. [10] first assessed the spatiotemporal pattern of Aβ-clearing after various anti-Aβ treatments. Interestingly, each anti-Aβ treatment showed a unique regiospecific efficacy, highlighting the spatial heterogeneity of the pathological progression of CNS disorders. By aligning these spatiotemporal Aβ-clearance profile with a previously established spatial-transcriptomic atlas, they further identified genes that may predict the efficacy of different anti-Aβ treatments. These results may thus guide the individualized therapeutics and future precision medicine for AD.

3.4. Understanding the molecular basis of neuronal communication

Brain exerts its function on the basis of complex communications between neurons, highlighting the significance of mapping neuronal connections in the brain and understanding their molecular basis. Chen et al. proposed a new technology named barcoded anatomy resolved by sequencing (BARseq) (Fig. 5) [81] via combining multiplexed analysis of projections by sequencing (MAPseq) [82] with BaristaSeq [60]. In MAPseq, short and random RNA barcodes are employed to uniquely label individual neurons. These barcodes can be transported into the axon terminal regions by MAPP-nλ, a modified presynaptic protein. Therefore, single neuron projection patterns can be read out through extracting and sequencing barcode mRNAs from the injection site and downstream targets of interest. Combining with these two methods, BARseq maps the projections of thousands of spatially resolved neurons in a single brain [81]. At first, the source region of the labeled neurons is injected with a viral library containing different barcode sequences. Then, BaristaSeq is performed at the injection site to read out the spatial barcodes in each neuron, and simultaneously the downstream areas are micro-dissected and sequenced via bulk RNA-seq. By employing BARseq, the authors not only recapitulated the well-known anatomical connectivity of auditory cortex but also revealed the gene expression pattern of neurons with distinct projections.

4. Mass spectrometry imaging (MSI) techniques

4.1. From mass spectrometry (MS) to MSI

MS is an analytical instrument that identifies ionized compounds based on their mass-to-charge ratio (m/z). A variety of methods are used for ionization including electrospray ionization (ESI), electron impact ionization (EI), atmospheric pressure chemical ionization (APCI), and matrix-assisted laser desorption/ionization (MALDI). Commercial MS instruments consist of four components: 1) an automatic sample handling system; 2) an ionization source (one of the aforementioned types) to generate the ionized molecules; 3) a mass analyzer, which may be triple quadrupole (QqQ), quadrupole ion trap (QTRAP), time-of-flight (TOF), Orbitrap, Fourier transform ion cyclotron resonance (FT-ICR), quadrupole-TOF (Q-TOF), or TOF/TOF; and 4) a mass detector to quantify the abundance of ions. MSI is a rapidly developing technology that can reveal the spatial distribution of molecules in tissue sections at cellular and subcellular levels. MSI were first introduced by Caprioli et al. [83] who employed MALDI-MSI to visualize large biomolecules in a rat pancreas section, hormone peptide in a rat pituitary section, and subcellular localization of protein molecules in 1997. Today, in addition to proteins/peptides measurement in spatial proteomics, the MSI technology has been able to detect metabolites such as neurotransmitters [84], amino acids [85], and fatty acids [86], lipids [87,88], and drugs [89] with spatial information in spatial metabolomics.

Similar to MS, MSI uses a focused ionization source (laser, charged droplets, ion source, etc.) to excite molecules in biological tissue slices point by point, and then to detect them in mass spectrometer. It is then possible, when all identified m/z points are integrated with the sample slide, to build 2D or 3D molecular

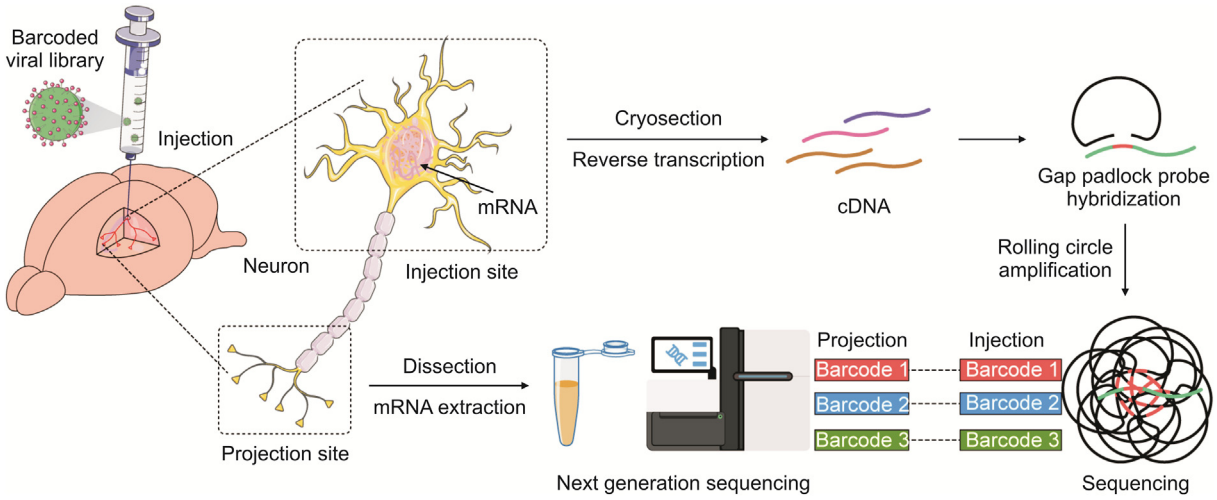

Fig. 5. The diagram of barcoded anatomy resolved by sequencing (BARseq). The source region of labeled neurons was injected with a viral library containing different barcode sequences. Then, barcode in situ targeted sequencing (BaristaSeq) is performed at injection site to read out the spatial barcodes in each neuron, and simultaneously the downstream areas are micro-dissected and sequenced by bulk RNA sequencing (RNA-seq). mRNA: messenger RNA; cDNA: complementary DNA.

maps. The probe-type MSI technique is classified in three types according to the ionization method used: 1) MALDI [90,91], which is capable of detecting large scale of chemicals, 2) secondary ion mass spectroscopy (SIMS) [90], with high sensitivity for element detection, and 3) constant pressure open ionized MSI technology, for instance the recently developed desorption electrospray ionization (DESI) (Fig. 6) [92]. In MALDI analysis, tissue sample is attached on a conductive plate followed by matrix coating. The mixture was shot by laser and then the analyte was induced to ionization via the energy transition from matrix. In SIMS analysis, tissue slide is attached on conductive plate without matrix. When the analyte in touch with high energy ion beams, primary ion and secondary ion bombarded and be measured in TOF mass analyzer on a regular basis. In DESI analysis, samples are mounted on a non-conductive surface and analyte is taken up by the charged solvent droplets directly which are captured by the mass spectrometer inlet. All these technologies show great application potential for spatially resolved proteomics and metabolomics.

The above mentioned MSI techniques have their own advantages: MALDI can be used for the detection of proteins and polypeptide molecules, but requires a relatively complex sample preparation process, whereas SIMS and DESI are suitable for the in situ detection of small molecules, and DESI is especially suitable for field detection. The MS ionization method has a great impact on the image resolution of MSI. The most widely used MALDI and DESI have an image spatial resolution of about 1–200 μm, far from the resolution of general optical imaging (28–500 nm), which limits the application of MSI technology.

4.2. MALDI

The process of MALDI-MSI includes tissue slice preparation, matrix embedding or coating, MS analysis, and image processing. First, matrix molecules are deposited symmetrically in tissue sections using sublimation, electrospray, difluidic atomization, or ultrasonic spray to promote ionization. The slices of the deposited matrix are sent into a mass spectrometer equipped with the MALDI ion source, and the sections are bombarded using a pulse laser of UV light. The energy absorbed by radiation is transferred to the point of organic matrix on the surface, molecules are ionized and subsequently analyzed by MS [93]. MALDI-MSI technology combines MS and scanning technology with computerized image processing software, providing a direct way to analyze biological groups and weaving slices to produce a 2D or 3D ion density map of arbitrarily specified compounds [94,95]. In MALDI imaging, the type of matrix, the process of matrix deposition, the parameters of the laser, and the performance of the mass spectrometer all affect the imaging quality [96]. MALDI-MSI high spatial resolution can reach the cellular level (<5 μm), furthermore, MALDI-MSI can detect a diverse array of biomolecules (e.g., metabolites and lipids) [97]. At present, commercial MALDI-MSI instruments have an analysis speed of up to 40 pixels/s, which greatly shortens the analysis time of MSI. MALDI-MSI's main limitations are the time-consuming pretreatment and the expensive fees required for laser maintenance. In general, the process of MALDI-MSI includes tissue slice making, matrix embedded or coating, MS analysis, and image processing.

4.3. SIMS

TOF-SIMS is a surface MS method in which the primary ions are directly irradiated with an accelerated ion beam, and the secondary ions generated are measured using a quadrupole mass spectrometer with TOF analyzer [98]. SIMS are popular in materials science to perform surface analysis of semiconductor materials and to profile semiconductor thin films made of inorganic material [99], but continued advancement in SIMS has expanded its application in the field of biology. At an early stage of the development of the SIMS method, Ga^+ and In^+ ionization sources were widely used [100]. The high excitation energy of these sources leads to dissociation of large biological molecules. Therefore, the use of SIMS was

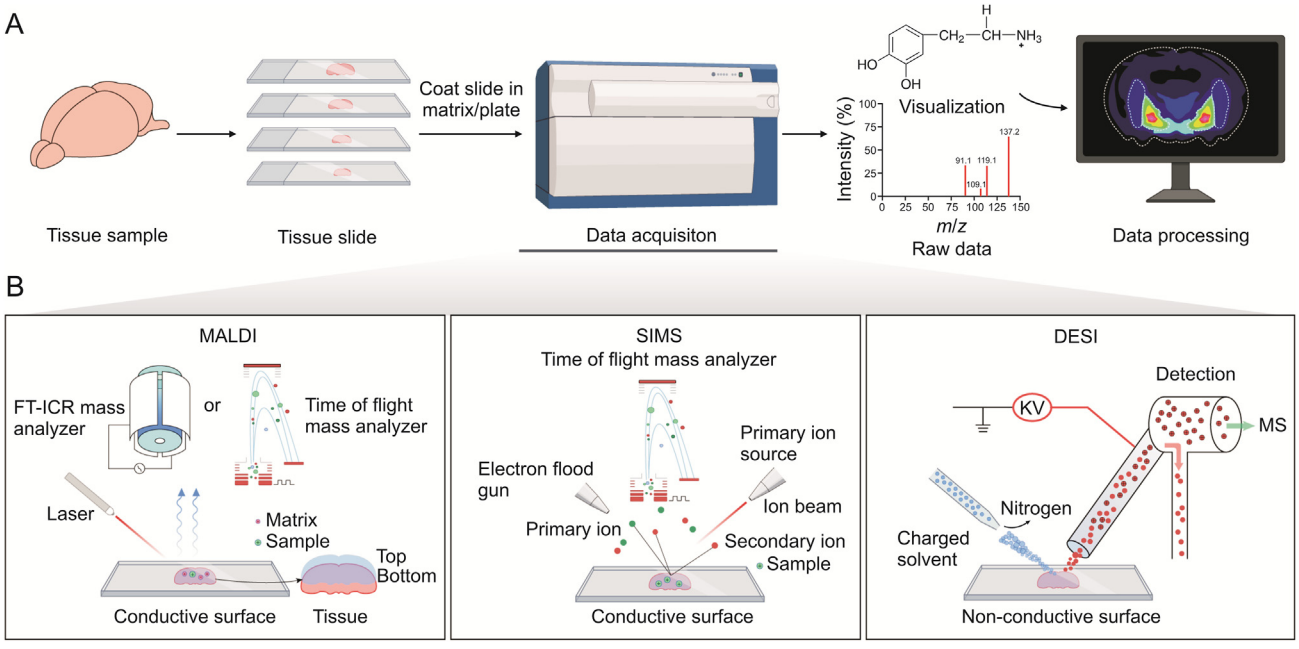

Fig. 6. The diagram of mass spectrometry imaging (MSI) technique. (A) General work flow of MSI. (B) Schematic illustration of ionizing mechanism in matrix assisted laser desorption ionization (MALDI), secondary ion mass spectroscopy (SIMS), and desorption electrospray ionization (DESI). *m*/*z*: mass-to-charge ratio; FT-ICR: Fourier transform ion cyclotron resonance; MS: mass spectrometry.

limited to the determination of compounds with molecular weight less than 200 Da only. More recently metal clusters ions and polyatomic ions have been introduced to SIMS systems to make the detection of larger molecules possible. Metal clusters ions like Au_x^+ and Bi_x^+ ($x = 1–7$) have the advantage of maintaining sub-micron image resolution while greatly improving the sensitivity for high molecular weight peptides and proteins. Polyatomic ions, like SF_5^+ and C_{60}^+, have the same sensitivity, but lower image resolution than metal clusters ions [101,102]. In general, gas cluster ion beams make TOF-SIMS imaging more practical for biological analysis. In addition, SIMS imaging methods processes are similar to MALDI-MSI, with the difference that the tissue slide can be used directly for SIMS analysis avoiding additional processing. However, the application of SIMS is still restricted by low intensity of MS/MS ions and the extensive fragmentation of molecular ions caused by the high energy ion beam.

4.4. DESI

Both MALDI-MSI and SIMS-MSI techniques generally require a vacuum environment. To overcome this limitation, Cooks et al. [103] developed DESI-MS under constant pressure. DESI sprays the solvent over an untreated tissue slide with the molecules on the surface, and is then dripped with more solvent to sputter the solution onto the mass spectrometer for ionization and analysis. This technique can be used on living samples or even in patients being operated on, and it has been successfully applied in clinical studies to recognize cancer and healthy tissues during cancers surgery in real time [104].

DESI is based on the droplet carrying mechanism. The spray solvent is first quickly atomized and accelerated by the high-speed nitrogen flow emitted from the atomizer tube. The charged droplets then hit the surface of the sample, turning the molecules sputtered to the gas phase with nitrogen purging and drying. Then, the charged droplets containing compounds are dissolved, captured, and eventually detected using a mass analyzer. DESI is similar to SIMS, except that in the former technique, compounds are dissociated at atmospheric pressure [105].

The quality and efficacy of DESI-MSI are greatly dependent on the solvent chosen at the spray stage. Moreover, distribution information of different compounds on the sample surface can be obtained by changing solvent systems. In addition, the distance and angle between the DESI nozzle, slide surface, and mass spectrum inlet can greatly influence the resolution and intensity of the m/z signal.

4.5. Sample preparation and data acquisition

The workflow of sample preparation of MSI is very different from standard MS. MSI is usually performed on flash-frozen tissue samples. This step is necessary to stop any cell reaction and enzyme-mediated molecular degradation in the tissue. The thickness of the tissue section for MSI usually ranges from 5 to 20 μm. In general, MALDI-MSI is used more often in metabolomics than proteomics. In contrast to metabolite imaging, the preparation process for protein MSI required additional in situ digestion steps by trypsin or other enzymes, because the lower molecular weight peptides are more prone to ionization than proteins and thus easier to detect via MS. A recent protocol for sample preparation has been optimized for trypsin concentration, digestion period, and matrix deposition to minimize ion inhibition and remove paraffin from the tissue [106]. After this step, those fresh sections are ready for DESI or SIMS analysis, while for MALDI-MSI, further coating samples with matrix is required for MALDI ionization. Frequently used MALDI matrixes to assist desorption and ionization include 2,6-dihydroxyacetophenone, 2,5-dihydroxybenzoic acid, 1,5-diaminonaphthalene, α-cyano-4-hydroxycinnamic acid, and sinapinic acid [107–111].

After optimization of the ion source parameters, tissue imaging is conducted on commercially available stages, such as the 2D automated Omni Spray source from Prosolia Inc. (Indianapolis, IN USA). Raw data, including stage time, position data, and spectra at each point, can be processed using software applications from the manufacturer or websites, such as BioMAP (www.maldi-msi.org).

4.6. MSI analysis of drug distribution

A major hurdle in CNS disease treatment is the delivery of therapeutic drugs to the target across the blood-brain barrier (BBB). Similarly, the efficacy of cancer chemotherapy drugs is limited by the blood-tumor barrier (BTB). Several groups have used MSI techniques to assess the target penetration of clinical drugs. For example, Tanaka et al. [109,112] used MALDI-MSI to quantify the spatial distribution of epertinib and lapatinib in brain and confirmed that when epertinib and lapatinib had the same concentrations at brain tumor position, plasma concentrations were significantly different at 4 h after oral administration. Another study using MALDI-MSI to determine the localization patterns of efavirenz, tenofovir, and emtricitabine in rat brain revealed that efavirenz concentration was high across the entire brain, whereas tenofovir was localized primarily in the cortex, and emtricitabine was distributed heterogeneously in the thalamus, corpus callosum, and hypothalamus [89]. These findings illustrate the advantages of MSI for monitoring drug delivery, providing not only the overall assessment of BBB or BTB permeability of drugs but also the distribution pattern within tissue. Further investigations may help guide the design of tissue-targeted drugs and explain the pharmacological and toxicological actions of some drugs.

5. MSI in CNS disorders

Before MSI technology was well established, brain tissues had to be anatomically separated for analysis of spatial heterogeneity. Due to difficulties in achieving anatomical precision, most of the research focused on whole brain tissue, whole hippocampal, cortex tissues, where monoamines, such as dopamine, noradrenaline, and serotonin, do not share the same alteration pattern. In addition, the results on neurotransmitters were not consistent across several studies using the same animal model and considering the same disease phase [113]. In contrast, MSI technology can directly reveal the spatial distributions of proteins, metabolites, lipids, and other molecules in brain tissues, thereby providing a more comprehensive explanation of the molecular mechanisms underlying neurodegenerative diseases.

5.1. MSI in neurodegenerative diseases

The detection of small molecule neurotransmitters and mapping of their spatial distributions are critical to the diagnosis and treatment of neurodegenerative diseases. How to accurately detect these molecules in situ and in brain sections is currently a significant topic in brain research. Shariatgorji et al. [114,115] developed a in situ derivatization approach based on MALDI-FT-ICR and MALDI-MSI for the simultaneous imaging and the absolute or relative quantification of multiple neurotransmitters such as dopamine, γ-amino butyric acid (GABA), glutamate and acetylcholine, neurotransmitter precursors such as β-*N*-

methylamino-L-alanine, and metabolites such as tyrosine, tryptamine, tyramine, and phenethylamine.

Protein aggregation is a pathological characteristic of many neurodegenerative diseases, and MSI can reveal the biogenesis of this process. Rohner et al. [116] performed MALDI-MSI analysis on brain tissue in AD model mice and identified five β-amyloid peptides and their spatial distributions. Results revealed that Aβ1–40 polypeptides were more abundant than other β-amyloid polypeptides, and are mainly distributed in the parietal bone, occipital cortex protrusion, and the lower part of the lateral sulcus. Kakuda et al. [117] similarly applied MALDI-MSI to study the distribution of different types of amyloid peptides the postmortem brains of in elderly adults suffering with AD and brain amyloid angiopathy. These MSI results showed that Aβ1–42 and Aβ1–43 peptides were deposited mainly in senile plaques in the brain, while Aβ1–36, Aβ1–37, Aβ1–38, Aβ1–39, Aβ1–40, and Aβ1–41 peptides were accumulated in the meninges, suggesting that Aβ polypeptides differentially contribute to AD pathogenesis, an idea that warrants further investigation.

In addition to Aβ, MALDI-MSI has also revealed the spatial distribution profile of AD relevant lipids. Kaya et al. [118] revealed that ceramide Cer (18:0), phosphatidylinositol PI (38:4), glucosinolate ST (24:0), lysophosphatidylcholine LPC (16:0), and LPC (18:0) were colocalized with β-amyloid polypeptide Aβ1–37, Aβ1–38, and Aβ1–40. Moreover, while ceramides were found to accumulate in β-amyloid plaques, ganglioside and sulfatide concentrations were lower in plaque regions. These results suggest that sphingolipid metabolism is involved in Aβ pathology or reparative mechanisms [119]. Hulme et al. [120] developed a method for high resolution neuropeptide imaging using a dry matrix that successfully revealed the detailed distribution patterns of Parkinson's disease (PD) molecules, such as enkephalin, acrophin, tachykinin, and neurohypotensin, across the whole brain of rats treated with 6-hydroxydopamine, highlighting the potential applications of the method in PD base research.

5.2. MSI in stroke

During cerebral ischemia, the supply of oxygen and glucose to the brain is restricted, and the concentrations of various metabolites involved in tricarboxylic acid cycle and mitochondrial activity change significantly. Liu et al. [121] employed MALDI-MSI to reveal the spatial specific distribution of molecules such as metal ions, amino acids, carboxylic acids, nucleotide derivatives, peptides, and lipids in rat brain subjected to an experimental ischemic stroke model. The amount of direct energy supply molecules (such as adenosine triphosphate, adenosine diphosphate, and adenosine monophosphate) was significantly reduced, while other metabolites (such as adenosine, creatinine, hypoxanthine, and creatine) were also decreased. Moreover, MALDI-MSI techniques have been employed in combination with liquid chromatography-tandem mass spectroscopy to analyze ischemia reperfusion induced alteration in the abundance of nucleic acids, such as uridine triphosphate, uridine monophosphate, uridine diphosphate, adenosine triphosphate, adenosine monophosphate, and adenosine diphosphate [122]. In addition, MALDI-MSI has been used to detect the impact of ischemia on the distribution and concentrations of lipids, including sulfatide (d18:1-C24h:0), phosphatidylcholines (PCs), and LysoPCs, in rat brain slices [87,88]. However, due to the limited resolution, instability of the matrix, lack of replicability, and insufficient molecular coverage, the spatial information of these lipid metabolites cannot fully explain cerebral ischemia mechanisms. However, with the development of technology and the integration of various disciplines, the pathogenesis of cerebral ischemia is yet to be gradually revealed.

5.3. MSI in CNS tumors

Surgery is a critical step in the treatment of brain tumors. Successful surgery requires complete removal of brain tumors to avoid recurrence, while causing minimal damage to normal brain tissues as much as possible. At present, it is difficult for conventional auxiliary imaging methods, such as magnetic resonance imaging (MRI), to distinguish tumor tissues from normal tissues in brain surgery. Tumor infiltration may exceed what can be seen on MRI images. These limitations lead to difficulties in safely removing tumors. Pathological staining methods are limited to samples with recognizable nucleic acid mutations, and it is hard to get metabolite-level or protein-level information. Human brain tissues are particularly rich in phospholipids, and these macromolecules are present in different concentrations in normal and tumor cells [123]. Fortunately, imaging of phospholipids in tissues using MSI technique to distinguish between normal and tumor tissues is now possible. As DESI-MSI works at constant pressure, which makes it a good choice for surgery applications. In 2013, Ebrlin et al. [124] successfully differentiated lipids between 15 gliomas and 8 meningioma samples using DESI-MSI combined with support vector machines and deep learning methods. In the meningioma samples, the main mass spectrum peaks were phosphatidylethanolamine, phosphatidylserine, and phosphatidylinositol, while thiosides were more abundance in gliomas. With 3D colocalization by DESI-MSI and MRI imaging, this method makes it possible to identify tumor boundaries and to classify similar tumors. Cooks and co-workers [125,126] developed a MasSpec Pen that provides localized molecular information from tissue samples based on the DESI technique. They modified the commercial DESI-MSI instrument so that it could be placed on the top of a cart as a separate system and it could be easily moved in the operating room. The surgeon removes the small biopsy, smears it on the glass, and analyzes it with the MasSpec Pen. After a few mins, MasSpec Pen tells the surgeon whether there are tumor cells in the tissue sample and estimates the penetration percentage of the tumor.

Several other key small molecules can also serve as specific biomarkers for tumors. Isocitrate dehydrogenase (IDH) mutations often occur in low grade gliomas and secondary glioblastomas [127], which enhance the conversion of citrate to 2-hydroxyglutaric acid (2-HG) [128]. The accumulation of 2-HG affects DNA methylation, prolyl hydrolase activity, cell growth regulation, and differentiation. While 2-HG is present in minimal concentration in normal cells, but it accumulates substantially in IDH1 and IDH2 mutant gliomas, thus 2-HG may represent a biomarker for IDH-mutant gliomas. Santagata et al. [129] used DESI-MSI to detect 2-HG in IDH1 mutation in glioma samples, and they found that the signal of 2-HG was positively correlated with tumor cell density. In a real-time surgical case, they imaged a glioma smear using DESI, combined with the stereogram of MRI. The co-location image clearly reveals the concentration of cancer cells present in the central and marginal areas of the tumor.

5.4. MSI in depression

Depression is one of the most prevalent and debilitating psychiatric disorders. Esteve et al. [130] applied MALDI-MSI to directly measure the altered amino neurotransmitters following experimentally induced cortical spreading depression (CSD) in mouse brain, and found a distinct expression pattern of inhibitory (GABA)

and excitatory (glutamate and aspartate) neurotransmitters in the mice cortex subjected to an experimental CSD model. Employing MALDI-MSI, Kleinridders et al. [131] revealed the region specific activity of glucose metabolism across the brain, which may shed light on depression pathology since it has been reported that fluctuating blood sugar levels in diabetes can predict brain dysfunctions, including depression [132,133].

6. Mass cytometry for targeted spatially resolved proteomics

In 2009, Tanner and co-workers from University of Toronto proposed the concept of mass cytometry first [134], and single cell mass cytometry by time-of-flight (CyTOF) has developed rapidly since this first report. Unlike traditional flow cytometry, mass cytometry using metal isotopes to label antibodies instead of fluorophore to overcome the overlapping between flow channels. In addition, mass cytometry uses inductively coupled plasma MS (ICP-MS) rather than lasers and photomultiplier tubes as detection, which greatly expands the number of detection channels. Based on these benefits, mass cytometry is a suitable tool in large scale immune monitoring, immunophenotyping, and classification of cell subpopulations. In CyTOF analysis, one area of interest in sample is collected and process into single cell suspension followed by incubation with metal-labeled antibody. Then, the labeled cell form droplets by going through a nebulizer and acquired by ICP-MS. Böttcher et al. [135] applied comprehensive single cell immune profiling of human microglia from different brain regions with mass cytometry. They drew the phenotypic characterization and confirmed the key transcriptomic signature of human microglia. Of note, in the subventricular zone and thalamus, a higher expression of markers involved in microglial activation.

These initial studies applied CyTOF to single cell suspensions without spatial information, while recent technologies known as multiplexed ion beam imaging (MIBI) and imaging mass cytometry (IMC) can characterize the spatial distribution of different cellular processes. In IMC strategy, metal labeled antibody is directly bound to targeted proteins in situ. With the help of laser gun, metals within the region of interest are released and subsequently detected by ICP-MS. Wang et al. [136] performed scRNA-seq combined with IMC on primary meningioma tumor samples to validate protein expression and reveal the spatial localization of protein markers. IMC can provide up to 50 antibodies (www.standardbio.com) conjugated to heavy metal isotopes related by autoimmune disease, whereby some researchers apply it at multiple sclerosis research. For instance, Park et al. [137] quantified 13 glial activation markers simultaneously in early and late acute multiple sclerosis brain lesions. Ramaglia et al. [138] characterized B cell and T cell subsets within the multiple sclerosis brain. Another promising variant of IMC is MIBI, which employs a similar process for sample preparation but uses SIMS coupled with TOF detector to achieve spatial distribution of highlight proteins. After the protein at slide sample stained with mantel-labeled antibodies, the complexes are sputtered by high energy ion beam and then detected by TOF spectrometer. By employing SIMS, Moon et al. [139] identified two AD-relevant clusters of proteins and located their positions.

7. Computational approaches for spatial-omics

While the volume and complexity of omics data is a major strength for studying the molecular mechanisms of disease, it also presents challenges for data presentation and interpretation. Here we provide an overview of the spatial omics data analysis toolkits in Table S2 [28,140–169] including the running environments, algorithms, and analytic methods for categorizing information. For transcriptomics analysis, there are several image segmentation algorithms based on deep learning models to construct spatial graphs, such as Stardist [170], Splinedist [171] and Cellpose [172]. With the spatial coordinates established in tissue atlas, the downstream toolkits provided a bunch of function such as differential gene expression between samples, cell types recognition, the spatial distribution of each cell type, and cell communication states based on ST datasets and H&E images, such as probabilistic cell typing by in situ sequencing (pciSeq) [149] and Seurat [148]. However, those toolkits could not interpret the ST data in single cell resolution. Several novel methods such as spatialDE [151], SPOTlight [145], spatial quantification of molecular data in python (Squidpy) [155], Giotto [157], and Cell2location [154] can carry out spatial sub clustering analysis of cell types and map scRNA-seq data with spatial data. However, they still fail to infer single cell data or bulk-seq data in situ directly. To fill this important gap, Liao et al. [147] set spatial transcriptomics as references and then map the bulk transcriptomes to the original section spatially with a single cell resolution with deep learning frameworks. Still, typical single cell transcriptomics does not include spatial coordinates let alone 3D spatial information. Zeira et al. [146] introduced probabilistic alignment of ST experiments (PASTE) using fused gromov-wasserstein optimal transport to align and integrate pairwise alignment of adjacent slices. PASTE visualize single cell RNA-seq data and ST data three dimensionally without additional histological images. It also provides a more representative ST slide by combining multiple slices into a “center”, which increases the representativeness relative to the independent analysis of individual slices [146]. Similar to PASTE, probabilistic embedding, clustering, and alignment for integrating spatial transcriptomics data (PRECAST) takes normalized gene expression matrices from multiple tissue slides as an input, then decomposes inputs into potential factors that present cell/domain types when performs spatial dimensionality reduction and spatial clustering, and eventually aligns scRNA-seq datasets by cell/domain types and spatial coordinates on multiple tissue slides [167].

A major problem in metabolomics and proteomics research is that raw data from different mass spectrometer brands are outputted in different formats. However, there are open source analysis software applications or pipelines available to address this issue (free software were listed on Table S2). Mainstream MSI manufacturers such as Bruker (SCiLS™ Lab) and Shimadzu (MALDI Solutions™) have launched their own commercial analysis software. The high price of commercial software for proteomics, such as PEAKS Studio (Bioinformatics Solutions Inc.), Progenesis QI (Waters Inc.), ProteinPilot (Sciex Inc.), and Proteome Discoverer (Thermo Fisher Scientific Inc.) prevents them from being widely practical.

The pipeline or software that can align full multi-omics datasets spatially has not been seen yet, while many computational methods are now available to integrate of the genome (methylome, chromatin accessibility), transcriptome, and proteome in single-cell resolution. Here, we classify the computational methods for multi-omics analysis into three types chronologically: 1) applied single omics analysis separately and manually annotate multi-omics data together; 2) computational integration of two omics data or more based on a different algorithm with or without spatial information; and 3) conjoint analysis of spatial transcriptome and proteome with DNA barcoded antibodies strategy in the same or neighbor section. We review those three types of multi-omics analysis with several cases in CNS.

7.1. Manual integrate single omics data together

Most of multi-omics study was applied single omics analysis separately. Grant et al. [173] integrated genomics with metabolomics to evaluate age at depressive onset on human plasma, with characterizing novel markers of major depressive disorder. Multi-omics integration network exposes four variants (in/near INTU, FAT1, CNTN6, and TM9SF2) and plasma metabolites (phosphatidylcholines, carnitines, biogenic amines, and amino acids) as biosignatures of early- and adult-onset major depressive disorder. Nativio et al. [26] integrated transcriptomic, proteomic, and epigenomic analyses of postmortem AD human brains to identify H3K27ac and H3K9ac genes affect late-onset AD pathways by dysregulating transcription-and chromatin-gene feedback. The histone acetyltransferases for H3K27ac and H3K9ac gene and protein showed an upregulation in both transcriptomic and proteomic analysis. Zhang et al. [27] analyzed proteomes and genomes of colon tumors and perform integrated proteogenomic analyses. They found that although copy number of mRNA abundance showed significant alterations, and the expression of related proteins is not necessarily altered. Their results call the attention to us that protein abundance may not be reliably reflected from mRNA-level at sometimes. This is the reason why we need to understand the information flow from DNA to protein to metabolite spatially and temporally when we decode physiopathological process in CNS.

7.2. Computational integrate single omics data together

The measurement of multiple data types (genome, transcriptome, proteome, metabolome, and modification omics) in the single cells has been developed. The computational integration of different data types is of great significance when synergistic infer the cell regulation network. Mainly, there are several algorithms were hired for integrative analysis of such data. For example, machine learning (single-cell aggregation and integration (scAI) [164], single-molecule fluorescence in situ hybridization with hidden Markov random field model (smfishhmrf) [156], and Giotto [157]), clustering model (spatial transcriptomics learn (stLearn) [153], Giotto [157], CiteFuse [162], and model-based analyses of single-cell transcriptome and regulome (MAESTRO) [161]), Bayesian model (bayesian random effects mixture model-single cell (BREM-SC) [166], multi-omics factor analysis (MOFA) and MOFA^{+} [165], and totalVI [163]), mutual nearest neighbors (spatially-resolved transcriptomics via epitope anchoring (STvEA) [159]), integrative non-negative matrix factorization (linked inference of genomic experimental relationships (LIGER) [169]), and generalized unsupervised manifold alignment (UnionCom) [168]. The integration of single omics data was able to find more differences that single-omics studies cannot provide. Cao et al. [168] applied scRNA-seq and scDNA-seq in breast cancer cells and found the discover clone-specific dysregulated biological pathways which cannot be outlined by either single omics data.

7.3. Conjoint analysis strategy based on DNA-barcoded antibodies

Although the computational integration of multi-omics builds the link between two or three omics data in single cells, the integration spatial-omics still in challenge. As we described before, DBiT-seq enabled high spatial resolution barcoding of mRNAs or proteins in mouse embryo [37]. Similar to DBiT-seq, spatial multi-omics (SM-Omics) combined spatial RNA-Seq with DNA-barcoded antibodies, antibody-based protein measurements, and immunofluorescence staining together. Different from DBiT-seq, SM-Omics induces liquid handler to achieve automatic and high throughput spatial RNA and protein measurements at the same time [174]. In another study using a similar paradigm, Govek et al. [159] developed a platform called STvEA based on the developed multiplex immunohistochemistry and cellular indexing of transcriptomes and epitopes by sequencing (CITE-seq) dataset with a shared antibody panel, which aims to mapping single-cell RNA-seq data and protein to the same images. Among these platforms, the DSP platform is commercially available and now widely used for multiomics of tumor microenvironment [36,175,176]. Unlike to DBiT-seq, SM-Omics and STvEA, DSP platform offers a custom RNA or protein plex with chosen target in situ and also apply for formalin-fixed and paraffin-embedded samples. Although high-throughput spatial omics have greatly improved our understanding of CNS diseases, acquiring the SM-Omics profile simultaneously in the same tissue or same section is still in the initial development stage. In general, SM-Omics research needs to be supported by more high spatial resolution instruments and more robust algorithms.

8. Future perspective of spatially resolved multi-omics

8.1. Joint application of spatially resolved multi-omics technologies in brain

We can find that the samples for different omics are usually derived from spatially adjacent tissue rather than the same piece of tissue. For example, after spatial transcriptomics analysis by ST, an adjacent region (<0.06 mm^3) on the identical brain slice can be isolated by LCM and goes through proteomics analysis by high-sensitivity MS [177]. Similarly, three consecutive slices can be analyzed by spatially resolved transcriptomics (Visium), metabolomics (MALDI-MSI), and proteomics (IMC), respectively [178]. Although these pioneer studies provide alternative approaches to multidimensionally assess the spatial heterogeneity of gene expression, the result inconsistency between proteins and nucleic acids, caused by the tiny spatial displacements, cannot be underestimated especially for brain. In general, non-target-based spatial multi-omics interaction analysis methods have not been reported yet. Before that, it is more urgent to define the tolerable error of spatial displacements when using adjacent tissue for multi-omics analysis.

8.2. Profile gene expression in neuronal projections in a whole-brain view

The nervous system is composed of different neural networks, each with its own connection mode, and axons can interact with thousands of cells in their neighborhood [179]. Numerous neurotransmitters (such as histamine and serotonin) can be released along the axons rather than only in terminus [180,181]. A detailed gene expression pattern along these neuronal projections may advance our knowledge of brain functions and illuminate the regulatory mechanisms underlying neurotransmission. BARseq has the ability to sequence and analyze the upstream brain region and some well-known downstream regions. However, so far, it cannot achieve gene profiling of neuronal projections in a whole-brain view. Fluorescence micro-optical sectioning tomography (fMOST) has been widely used in neuroscience to three-dimensionally visualize neuronal projections of the whole brain [182,183]. So far, single-cell RNA-seq has been employed parallelly with fMOST to confirm the cell clustering in a given region [184]. The combination of fMOST or similar technology with ISS may be worth expecting for this purpose.

8.3. Application of the spatial multi-omics in living cells and organoids

Neuronal activity is highly dynamic and the molecular basis of brain functions like consciousness and cognition is barely known. Cutting-edge technologies have achieved the single-cell resolved imaging of intracellular calcium spark and thus tracking the activities of hundreds of neurons simultaneously in awake, behaving animals [185,186]. So, is it possible to track "the spark of thought" in the transcriptomic or proteomic level? Unfortunately, there is currently no spatial-omics technology that can be used for live cells ex vivo or in vivo. Many researchers have performed spatial omics analysis through human organotypic slices [177,178], but these molecular profiles only represent a single snapshot within the tissue and cannot track the transcription activity of a living cell in a time-lapse. How to achieve living omics research is still an unanswered question. In 2017, Pei et al. [187] developed a new approach (Polylox) to generate 1.8 million endogenous DNA barcodes in vivo allowing single-cell labeling in a non-invasive way. These results have laid a solid foundation for future multi-omics assay in living cells.

It must also be noted that clinical samples are valuable and difficult to obtain. Human organoids provide an alternative choice for clinical research. Organoids are small-scale constructs derived from patients' stem cells or biopsies that recapitulate key molecular and structural characteristics of their tissue of origin [188]. In 2005 and 2007, Watanabe et al. [189,190] taken the lead in developing a 3D culture of different brain regions from mouse or human pluripotent stem cells to restructure brain organoids. After that, Bakker et al. [191] developed a BBB organoid platform for drug analysis by fluorescent microscopy and MALDI-MSI. Spruill et al. [192] first examined small molecules by MALDI-TOF from 16-day-old and 36-day-old brain organoids which were populated solely with neuroprogenitors. Recently, Bakker et al. [191] described an MSI protocol specifically focusing on the collecting and embedding of the organoids, and give recommendations for MSI-specific sample preparation, data acquisition, and molecular identification by tandem MS. Therefore, MSI study at brain organoids provides an opportunity to picture the metabolites/proteins-altas dynamically during the CNS development, especially when human brain samples are hard to obtain in anytime stage [188–192].

8.4. Joint application of MSI and other imaging technique

The application of MSI has been greatly limited by its unsatisfying spatial resolution. The integrative application of MSI and other imaging techniques may be a way out. Laser scanning confocal microscopes can provide quantitative and real-time observation of the subcellular structure in living cells. With the help of confocal microscopes, label-free MSI strategy offers numerous candidate targets at cellular and subcellular level for research fields such as cell biology and drug discovery. Passarelli et al. [193] developed a 3D OrbiSIMS method to construct 3D distribution of metabolites at subcellular resolution. Proetto et al. [194] established a least squares conformal maps (LSCM) and nanoscale SIMS (NanoSIMS) combined imaging analysis platform, which reveals in situ the intracellular drug release process of oxaliplatin with self-assembled polymer nanomaterials. Orphan et al. [195] employed FISH approach to label and locate specific bacterial polymerizers in cells, and at the same time they have combined NanoSIMS in situ imaging to quantify the different uptaking efficiency of ^{12}C-labeled carbon sources, ^{13}C-labeled carbon sources, and ^{15}N-labeled nitrogen sources among several bacteria. The results of these studies demonstrate the great potential of FISH-MSI and LSCM-MSI for the study of cell biology, drug discovery and of the complex responses of drugs and organs from on-target and off-target engagement.

8.5. Further functional verification and clinical translation

Although lots of studies have introduced spatially resolved multi-omics technologies to uncover novel drug targets for CNS disorders, few targets are further verified by functional assays. Since these technologies emphasize the spatial heterogeneity of the brain, the combination of other spatiotemporally specific technologies, (such as Cre-Loxp recombination and optogenetics/chemogenetics) is necessary to promise an unbiased assessment. In addition, those molecules with spatially specific distribution may not only serve as drug targets but also target drugs to the selected area. By combining materials science, spatially resolved multi-omics data may illuminate precise treatment for CNS disorders by targeting drugs to certain molecule-enriched cell subpopulation or brain region.

9. Conclusion

Spatial multi-omics offers a novel perspective to reveal the functional heterogeneity of the brain. It is expected to build the spatial atlas of the brain, decipher the CNS disorders, and decipher neuronal communication through the combination of spatial multi-omics technologies. Here we review the main approaches and computational algorithms of spatial transcriptomics, proteomics, and metabolomics. Moreover, the integration method developed in recent years between omics datasets has been summarized above. Spatial multi-omics have shown its power in deciphering both physical and pathological events in the brain. However, there are still many problems that need to be addressed. In addition to the above-mentioned challenges, almost all spatially resolved multi-omics technologies are expensive and time-consuming. There is still a long way to go to popularize these technologies. Despite the limitations, spatially resolved multi-omics technologies have undoubtedly widened our understanding of the brain's spatial heterogeneity. In the future, spatially resolved multi-omics will promote neuroscience research and shed light on the therapeutic strategies for CNS disorders.

CRediT author statement

Yijia Fangma and **Mengting Liu:** Conceptualization, Methodology, Writing - Original draft preparation; **Jie Liao:** Visualization, Data curation, Writing - Reviewing and Editing; **Zhong Chen** and **Yanrong Zheng:** Supervision, Project administration, Funding acquisition, Writing - Reviewing and Editing.

Declaration of competing interest

The authors declare that there are no conflicts of interest.

Acknowledgments

This work was supported by the National Natural Science Foundation of China (Grant Nos.: U21A20418, 82003727, and 82273903), and Zhejiang Provincial Natural Science Foundation, China (Grant No.: LQ21H310002).

Appendix A. Supplementary data

Supplementary data to this article can be found online at https://doi.org/10.1016/j.jpha.2023.04.003.

References

[1] J. Liao, X. Lu, X. Shao, et al., Uncovering an organ's molecular architecture at single-cell resolution by spatially resolved transcriptomics, Trends Biotechnol. 39 (2021) 43–58.
[2] E. Miyoshi, V. Swarup, Rogue gene networks gone awry in Alzheimer's disease, Neural Regen. Res. 16 (2021) 2415–2416.
[3] M. Zhang, S.W. Eichhorn, B. Zingg, et al., Spatially resolved cell atlas of the mouse primary motor cortex by MERFISH, Nature 598 (2021) 137–143.
[4] C.A. Moreau, A. Raznahan, P. Bellec, et al., Dissecting autism and schizophrenia through neuroimaging genomics, Brain 144 (2021) 1943–1957.
[5] M. Wang, W.M. Song, C. Ming, et al., Guidelines for bioinformatics of single-cell sequencing data analysis in Alzheimer's disease: Review, recommendation, implementation and application, Mol. Neurodegener. 17 (2022), 17.
[6] Y. Fan, Z. Chen, M. Zhang, Role of exosomes in the pathogenesis, diagnosis, and treatment of central nervous system diseases, J. Transl. Med. 20 (2022), 291.
[7] D.E. Tylawsky, H. Kiguchi, J. Vaynshteyn, et al., P-selectin-targeted nanocarriers induce active crossing of the blood-brain barrier via caveolin-1-dependent transcytosis, Nat. Mater. 22 (2023) 391–399.
[8] Y. Ren, Z. Huang, L. Zhou, et al., Spatial transcriptomics reveals niche-specific enrichment and vulnerabilities of radial glial stem-like cells in malignant gliomas, Nat. Commun. 14 (2023), 1028.
[9] A.L. Ji, A.J. Rubin, K. Thrane, et al., Multimodal analysis of composition and spatial architecture in human squamous cell carcinoma, Cell 182 (2020) 1661–1662.
[10] D. Kirschenbaum, E. Dadgar-Kiani, F. Catto, et al., Whole-brain microscopy reveals distinct temporal and spatial efficacy of anti-Aβ therapies, EMBO Mol. Med. 15 (2023), e16789.
[11] G.C. Bingham, F. Lee, A. Naba, et al., Spatial-omics: Novel approaches to probe cell heterogeneity and extracellular matrix biology, Matrix Biol. 91–92 (2020) 152–166.
[12] C.G. Williams, H.J. Lee, T. Asatsuma, et al., An introduction to spatial transcriptomics for biomedical research, Genome Med. 14 (2022), 68.
[13] J.F. Navarro, D.L. Croteau, A. Jurek, et al., Spatial transcriptomics reveals genes associated with dysregulated mitochondrial functions and stress signaling in Alzheimer disease, iScience 23 (2020), 101556.
[14] W.-T. Chen, A. Lu, K. Craessaerts, et al., Spatial transcriptomics and *in situ* sequencing to study Alzheimer's disease, Cell 182 (2020) 976–991.e19.
[15] K.R. Maynard, L. Collado-Torres, L.M. Weber, et al., Transcriptome-scale spatial gene expression in the human dorsolateral prefrontal cortex, Nat. Neurosci. 24 (2021) 425–436.
[16] J.S. Sadick, M.R. O'Dea, P. Hasel, et al., Astrocytes and oligodendrocytes undergo subtype-specific transcriptional changes in Alzheimer's disease, Neuron 110 (2022) 1788–1805.e10.
[17] X. Wei, S. Fu, H. Li, et al., Single-cell Stereo-seq reveals induced progenitor cells involved in axolotl brain regeneration, Science 377 (2022), eabp9444.
[18] M. Eisenstein, Seven technologies to watch in 2022, Nature 601 (2022) 658–661.
[19] T.G. Evans, Considerations for the use of transcriptomics in identifying the "genes that matter" for environmental adaptation, J. Exp. Biol. 218 (2015) 1925–1935.
[20] C.A. Waudby, C.M. Dobson, J. Christodoulou, Nature and regulation of protein folding on the ribosome, Trends Biochem. Sci. 44 (2019) 914–926.
[21] L.C. Czuba, K.M. Hillgren, P.W. Swaan, Post-translational modifications of transporters, Pharmacol. Ther. 192 (2018) 88–99.
[22] N.T. Ingolia, J.A. Hussmann, J.S. Weissman, Ribosome profiling: Global views of translation, Cold Spring. Harb. Perspect. Biol. 11 (2019), a032698.
[23] S.F. Nassar, K. Raddassi, T. Wu, Single-cell multiomics analysis for drug discovery, Metabolites 11 (2021), 729.
[24] D.M. Lovinger, Communication networks in the brain: Neurons, receptors, neurotransmitters, and alcohol, Alcohol Res. Health 31 (2008) 196–214.
[25] S.E. Hyman, Neurotransmitters, Curr. Biol. 15 (2005) R154–R158.
[26] R. Nativio, Y. Lan, G. Donahue, et al., An integrated multi-omics approach identifies epigenetic alterations associated with Alzheimer's disease, Nat. Genet. 52 (2020) 1024–1035.
[27] B. Zhang, J. Wang, X. Wang, et al., Proteogenomic characterization of human colon and rectal cancer, Nature 513 (2014) 382–387.
[28] K.R. Campbell, A. Steif, E. Laks, et al., clonealign: Statistical integration of independent single-cell RNA and DNA sequencing data from human cancers, Genome Biol. 20 (2019), 54.
[29] L. Moses, L. Pachter, Museum of spatial transcriptomics, Nat. Methods 19 (2022) 534–546.
[30] P. Civita, S. Franceschi, P. Aretini, et al., Laser capture microdissection and RNA-seq analysis: High sensitivity approaches to explain histopathological heterogeneity in human glioblastoma FFPE archived tissues, Front. Oncol. 9 (2019), 482.
[31] G. Peng, S. Suo, J. Chen, et al., Spatial transcriptome for the molecular annotation of lineage fates and cell identity in mid-gastrula mouse embryo, Dev. Cell 36 (2016) 681–697.
[32] J. Chen, S. Suo, P.P. Tam, et al., Spatial transcriptomic analysis of cryosectioned tissue samples with Geo-seq, Nat. Protoc. 12 (2017) 566–580.
[33] J.P. Junker, E.S. Noël, V. Guryev, et al., Genome-wide RNA tomography in the zebrafish embryo, Cell 159 (2014) 662–675.
[34] Y. Lee, D. Bogdanoff, Y. Wang, et al., XYZeq: Spatially resolved single-cell RNA sequencing reveals expression heterogeneity in the tumor microenvironment, Sci. Adv. 7 (2021), eabg4755.
[35] J.M. Beechem, High-plex spatially resolved RNA and protein detection using digital spatial profiling: A technology designed for immuno-oncology biomarker discovery and translational research, Methods Mol. Biol. 2055 (2020) 563–583.
[36] C.R. Merritt, G.T. Ong, S.E. Church, et al., Multiplex digital spatial profiling of proteins and RNA in fixed tissue, Nat. Biotechnol. 38 (2020) 586–599.
[37] Y. Liu, M. Yang, Y. Deng, et al., High-spatial-resolution multi-omics sequencing via deterministic barcoding in tissue, Cell 183 (2020) 1665–1681.e18.
[38] P.L. Ståhl, F. Salmén, S. Vickovic, et al., Visualization and analysis of gene expression in tissue sections by spatial transcriptomics, Science 353 (2016) 78–82.
[39] N. Wang, X. Li, R. Wang, et al., Spatial transcriptomics and proteomics technologies for deconvoluting the tumor microenvironment, Biotechnol. J. 16 (2021), e2100041.
[40] E.E. Dixon, H. Wu, Y. Muto, et al., Spatially resolved transcriptomic analysis of acute kidney injury in a female murine model, J. Am. Soc. Nephrol. 33 (2022) 279–289.
[41] S.G. Rodriques, R.R. Stickels, A. Goeva, et al., Slide-seq: A scalable technology for measuring genome-wide expression at high spatial resolution, Science 363 (2019) 1463–1467.
[42] S. Vickovic, G. Eraslan, F. Salmén, et al., High-definition spatial transcriptomics for *in situ* tissue profiling, Nat. Methods 16 (2019) 987–990.
[43] S.R. Srivatsan, J.L. McFaline-Figueroa, V. Ramani, et al., Massively multiplex chemical transcriptomics at single-cell resolution, Science 367 (2020) 45–51.
[44] S.R. Srivatsan, M.C. Regier, E. Barkan, et al., Embryo-scale, single-cell spatial transcriptomics, Science 373 (2021) 111–117.
[45] A. Chen, S. Liao, M. Cheng, et al., Spatiotemporal transcriptomic atlas of mouse organogenesis using DNA nanoball-patterned arrays, Cell 185 (2022) 1777–1792.e21.
[46] R. Drmanac, A.B. Sparks, M.J. Callow, et al., Human genome sequencing using unchained base reads on self-assembling DNA nanoarrays, Science 327 (2010) 78–81.
[47] A. Raj, P. van den Bogaard, S.A. Rifkin, et al., Imaging individual mRNA molecules using multiple singly labeled probes, Nat. Methods 5 (2008) 877–879.
[48] K.H. Chen, A.N. Boettiger, J.R. Moffitt, et al., RNA imaging. Spatially resolved, highly multiplexed RNA profiling in single cells, Science 348 (2015), aaa6090.
[49] J.R. Moffitt, D. Bambah-Mukku, S.W. Eichhorn, et al., Molecular, spatial, and functional single-cell profiling of the hypothalamic preoptic region, Science 362 (2018), eaau5324.
[50] R. Fang, C. Xia, J.L. Close, et al., Conservation and divergence of cortical cell organization in human and mouse revealed by MERFISH, Science 377 (2022) 56–62.
[51] C. Xia, J. Fan, G. Emanuel, et al., Spatial transcriptome profiling by MERFISH reveals subcellular RNA compartmentalization and cell cycle-dependent gene expression, Proc. Natl. Acad. Sci. U S A 116 (2019) 19490–19499.
[52] G. Wang, J.R. Moffitt, X. Zhuang, Multiplexed imaging of high-density libraries of RNAs with MERFISH and expansion microscopy, Sci. Rep. 8 (2018), 4847.
[53] E. Lubeck, A.F. Coskun, T. Zhiyentayev, et al., Single-cell *in situ* RNA profiling by sequential hybridization, Nat. Methods 11 (2014) 360–361.
[54] E. Lubeck, L. Cai, Single-cell systems biology by super-resolution imaging and combinatorial labeling, Nat. Methods 9 (2012) 743–748.
[55] C.L. Eng, M. Lawson, Q. Zhu, et al., Transcriptome-scale super-resolved imaging in tissues by RNA seqFISH, Nature 568 (2019) 235–239.
[56] M.J. Levesque, P. Ginart, Y. Wei, et al., Visualizing SNVs to quantify allele-specific expression in single cells, Nat. Methods 10 (2013) 865–867.
[57] M.J. Levesque, A. Raj, Single-chromosome transcriptional profiling reveals chromosomal gene expression regulation, Nat. Methods 10 (2013) 246–248.
[58] X. Wang, W.E. Allen, M.A. Wright, et al., Three-dimensional intact-tissue sequencing of single-cell transcriptional states, Science 361 (2018), eaat5691.
[59] R. Ke, M. Mignardi, A. Pacureanu, et al., *In situ* sequencing for RNA analysis in preserved tissue and cells, Nat, Methods 10 (2013) 857–860.
[60] X. Chen, Y.C. Sun, G.M. Church, et al., Efficient *in situ* barcode sequencing using padlock probe-based BaristaSeq, Nucleic Acids Res. 46 (2018), e22.
[61] J.H. Lee, E.R. Daugharthy, J. Scheiman, et al., Fluorescent *in situ* sequencing (FISSEQ) of RNA for gene expression profiling in intact cells and tissues, Nat. Protoc. 10 (2015) 442–458.
[62] S. Alon, D.R. Goodwin, A. Sinha, et al., Expansion sequencing: Spatially precise *in situ* transcriptomics in intact biological systems, Science 371 (2021), eaax2656.
[63] C. Ortiz, J.F. Navarro, A. Jurek, et al., Molecular atlas of the adult mouse brain, Sci. Adv. 6 (2020), eabb3446.

[64] P. Hasel, I.V.L. Rose, J.S. Sadick, et al., Neuroinflammatory astrocyte subtypes in the mouse brain, Nat. Neurosci. 24 (2021) 1475–1487.
[65] H. Keren-Shaul, A. Spinrad, A. Weiner, et al., A unique microglia type associated with restricting development of Alzheimer's disease, Cell 169 (2017) 1276–1290.e17.
[66] S. Zechel, P. Zajac, P. Lönnerberg, et al., Topographical transcriptome mapping of the mouse medial ganglionic eminence by spatially resolved RNA-seq, Genome Biol. 15 (2014), 486..
[67] S. Shah, E. Lubeck, W. Zhou, et al., *In situ* transcription profiling of single cells reveals spatial organization of cells in the mouse hippocampus, Neuron 92 (2016) 342–357.
[68] C.C. Xiang, E. Mezey, M. Chen, et al., Using DSP, a reversible cross-linker, to fix tissue sections for immunostaining, microdissection and expression profiling, Nucleic Acids Res. 32 (2004), e185.
[69] M. Menzel, J.A. Reuter, D. Gräßel, et al., Scattered Light Imaging: Resolving the substructure of nerve fiber crossings in whole brain sections with micrometer resolution, Neuroimage 233 (2021), 117952.
[70] D. Tavares-Ferreira, S. Shiers, P.R. Ray, et al., Spatial transcriptomics of dorsal root ganglia identifies molecular signatures of human nociceptors, Sci. Transl. Med. 14 (2022), eabj8186.
[71] K.A. Aldinger, Z. Thomson, I.G. Phelps, et al., Spatial and cell type transcriptional landscape of human cerebellar development, Nat. Neurosci. 24 (2021) 1163–1175.
[72] B. D'Orsi, J. Mateyka, J.H.M. Prehn, Control of mitochondrial physiology and cell death by the Bcl-2 family proteins Bax and Bok, Neurochem. Int. 109 (2017) 162–170.
[73] J.J. Schulman, L.M. Szczesniak, E.N. Bunker, et al., Bok regulates mitochondrial fusion and morphology, Cell Death Differ. 26 (2019) 2682–2694.
[74] R.H. Swerdlow, Mitochondria and mitochondrial cascades in Alzheimer's disease, J. Alzheimers Dis. 62 (2018) 1403–1416.
[75] S. Maniatis, T. Äijö, S. Vickovic, et al., Spatiotemporal dynamics of molecular pathology in amyotrophic lateral sclerosis, Science 364 (2019) 89–93.
[76] J.C. Dodge, C.M. Treleaven, J. Pacheco, et al., Glycosphingolipids are modulators of disease pathogenesis in amyotrophic lateral sclerosis, Proc. Natl. Acad. Sci. U S A 112 (2015) 8100–8105.
[77] X. Xu, A. Denic, L.R. Jordan, et al., A natural human IgM that binds to gangliosides is therapeutic in murine models of amyotrophic lateral sclerosis, Dis. Model. Mech. 8 (2015) 831–842.
[78] J.M. Gregory, K. McDade, M.R. Livesey, et al., Spatial transcriptomics identifies spatially dysregulated expression of GRM3 and USP47 in amyotrophic lateral sclerosis, Neuropathol. Appl. Neurobiol. 46 (2020) 441–457.
[79] M.G. Filbin, I. Tirosh, V. Hovestadt, et al., Developmental and oncogenic programs in H3K27M gliomas dissected by single-cell RNA-seq, Science 360 (2018) 331–335.
[80] C.P. Couturier, S. Ayyadhury, P.U. Le, et al., Single-cell RNA-seq reveals that glioblastoma recapitulates a normal neurodevelopmental hierarchy, Nat. Commun. 11 (2020), 3406.
[81] X. Chen, Y.C. Sun, H. Zhan, et al., High-throughput mapping of long-range neuronal projection using *in situ* sequencing, Cell 179 (2019) 772–786.e19.
[82] J.M. Kebschull, P. Garcia da Silva, A.P. Reid, et al., High-throughput mapping of single-neuron projections by sequencing of barcoded RNA, Neuron 91 (2016) 975–987.
[83] R.M. Caprioli, T.B. Farmer, J. Gile, Molecular imaging of biological samples: Localization of peptides and proteins using MALDI-TOF MS, Anal. Chem. 69 (1997) 4751–4760.
[84] A. Midey, H. Olivos, B. Shrestha, Spatial mapping of cellular metabolites using DESI ion mobility mass spectrometry, Methods Mol. Biol. 2064 (2020) 181–190.
[85] J.G. Swales, A. Dexter, G. Hamm, et al., Quantitation of endogenous metabolites in mouse tumors using mass-spectrometry imaging, Anal. Chem. 90 (2018) 6051–6058.
[86] G. Wang, B. Heijs, S. Kostidis, et al., Spatial dynamic metabolomics identifies metabolic cell fate trajectories in human kidney differentiation, Cell Stem Cell 29 (2022) 1580–1593.e7.
[87] H.Y. Wang, H.W. Wu, P.J. Tsai, et al., MALDI-mass spectrometry imaging of desalted rat brain sections reveals ischemia-mediated changes of lipids, Anal. Bioanal. Chem. 404 (2012) 113–124.
[88] D. Miura, Y. Fujimura, M. Yamato, et al., Ultrahighly sensitive *in situ* metabolomic imaging for visualizing spatiotemporal metabolic behaviors, Anal. Chem. 82 (2010) 9789–9796.
[89] S. Ntshangase, S. Mdanda, S.D. Singh, et al., Mass spectrometry imaging demonstrates the regional brain distribution patterns of three first-line antiretroviral drugs, ACS Omega 4 (2019) 21169–21177.
[90] P.J. Todd, T.G. Schaaff, P. Chaurand, et al., Organic ion imaging of biological tissue with secondary ion mass spectrometry and matrix-assisted laser desorption/ionization, J. Mass Spectrom. 36 (2001) 355–369.
[91] M. Stoeckli, P. Chaurand, D.E. Hallahan, et al., Imaging mass spectrometry: A new technology for the analysis of protein expression in mammalian tissues, Nat. Med. 7 (2001) 493–496.
[92] J.M. Wiseman, D.R. Ifa, Q. Song, et al., Tissue imaging at atmospheric pressure using desorption electrospray ionization (DESI) mass spectrometry, Angew. Chem. Int. Ed. Engl. 45 (2006) 7188–7192.
[93] A. Doerr, Mass spectrometry imaging takes off, Nat. Methods 15 (2018), 32.
[94] M. Kompauer, S. Heiles, B. Spengler, Atmospheric pressure MALDI mass spectrometry imaging of tissues and cells at 1.4-μm lateral resolution, Nat. Methods 14 (2017) 90–96.
[95] M. Kompauer, S. Heiles, B. Spengler, Autofocusing MALDI mass spectrometry imaging of tissue sections and 3D chemical topography of nonflat surfaces, Nat. Methods 14 (2017) 1156–1158.
[96] J.L. Norris, R.M. Caprioli, Analysis of tissue specimens by matrix-assisted laser desorption/ionization imaging mass spectrometry in biological and clinical research, Chem. Rev. 113 (2013) 2309–2342.
[97] N. Ogrinc Potočnik, T. Porta, M. Becker, et al., Use of advantageous, volatile matrices enabled by next-generation high-speed matrix-assisted laser desorption/ionization time-of-flight imaging employing a scanning laser beam, Rapid Commun. Mass Spectrom. 29 (2015) 2195–2203.
[98] J.S. Fletcher, J.C. Vickerman, N. Winograd, Label free biochemical 2D and 3D imaging using secondary ion mass spectrometry, Curr. Opin. Chem. Biol. 15 (2011) 733–740.
[99] S. Ninomiya, K. Ichiki, H. Yamada, et al., Molecular depth profiling of multilayer structures of organic semiconductor materials by secondary ion mass spectrometry with large argon cluster ion beams, Rapid Commun. Mass Spectrom. 23 (2009) 3264–3268.
[100] J.S. Fletcher, J.C. Vickerman, Secondary ion mass spectrometry: Characterizing complex samples in two and three dimensions, Anal. Chem. 85 (2013) 610–639.
[101] E.A. Jones, N.P. Lockyer, J.C. Vickerman, Depth profiling brain tissue sections with a 40 keV C_{60}^+ primary ion beam, Anal. Chem. 80 (2008) 2125–2132.
[102] N. Davies, D.E. Weibel, P. Blenkinsopp, et al., Development and experimental application of a gold liquid metal ion source, Appl. Surf. Sci. 203–204 (2003) 223–227.
[103] R.G. Cooks, Z. Ouyang, Z. Takats, et al., Detection technologies. Ambient mass spectrometry, Science 311 (2006) 1566–1570.
[104] K. Chan, P. Lanthier, X. Liu, et al., MALDI mass spectrometry imaging of gangliosides in mouse brain using ionic liquid matrix, Anal. Chim. Acta 639 (2009) 57–61.
[105] Z. Takáts, J.M. Wiseman, R.G. Cooks, Ambient mass spectrometry using desorption electrospray ionization (DESI): Instrumentation, mechanisms and applications in forensics, chemistry, and biology, J. Mass Spectrom. 40 (2005) 1261–1275.
[106] J. Hermann, H. Noels, W. Theelen, et al., Sample preparation of formalin-fixed paraffin-embedded tissue sections for MALDI-mass spectrometry imaging, Anal. Bioanal. Chem. 412 (2020) 1263–1275.
[107] E.H. Seeley, S.R. Oppenheimer, D. Mi, et al., Enhancement of protein sensitivity for MALDI imaging mass spectrometry after chemical treatment of tissue sections, J. Am. Soc. Mass Spectrom. 19 (2008) 1069–1077.
[108] Y. Chen, W. Tang, A. Gordon, et al., Development of an integrated tissue pretreatment protocol for enhanced MALDI MS imaging of drug distribution in the brain, J. Am. Soc. Mass Spectrom. 31 (2020) 1066–1073.
[109] Y. Tanaka, M. Hirata, S. Shinonome, et al., Distribution analysis of epertinib in brain metastasis of HER2-positive breast cancer by imaging mass spectrometry and prospect for antitumor activity, Sci. Rep. 8 (2018), 343.
[110] Š. Strnad, V. Pražienková, D. Sýkora, et al., The use of 1,5-diaminonaphthalene for matrix-assisted laser desorption/ionization mass spectrometry imaging of brain in neurodegenerative disorders, Talanta 201 (2019) 364–372.
[111] E.R. van Hove, D.F. Smith, L. Fornai, et al., An alternative paper based tissue washing method for mass spectrometry imaging: Localized washing and fragile tissue analysis, J. Am. Soc. Mass Spectrom. 22 (2011) 1885–1890.
[112] H. Tanaka, M. Hirata, S. Shinonome, et al., Preclinical antitumor activity of S-222611, an oral reversible tyrosine kinase inhibitor of epidermal growth factor receptor and human epidermal growth factor receptor 2, Cancer Sci. 105 (2014) 1040–1048.
[113] M. Liu, L. Tang, X. Liu, et al., An evidence-based review of related metabolites and metabolic network research on cerebral ischemia, Oxid. Med. Cell. Longev. 2016 (2016), 9162074.
[114] M. Shariatgorji, A. Nilsson, P. Källback, et al., Pyrylium salts as reactive matrices for MALDI-MS imaging of biologically active primary amines, J. Am. Soc. Mass Spectrom. 26 (2015) 934–939.
[115] M. Shariatgorji, A. Nilsson, R.J. Goodwin, et al., Direct targeted quantitative molecular imaging of neurotransmitters in brain tissue sections, Neuron 84 (2014) 697–707.
[116] T.C. Rohner, D. Staab, M. Stoeckli, MALDI mass spectrometric imaging of biological tissue sections, Mech. Ageing Dev. 126 (2005) 177–185.
[117] N. Kakuda, T. Miyasaka, N. Iwasaki, et al., Distinct deposition of amyloid-β species in brains with Alzheimer's disease pathology visualized with MALDI imaging mass spectrometry, Acta Neuropathol. Commun. 5 (2017), 73.
[118] I. Kaya, D. Brinet, W. Michno, et al., Novel trimodal MALDI imaging mass spectrometry (IMS3) at 10 μm reveals spatial lipid and peptide correlates implicated in Aβ plaque pathology in Alzheimer's disease, ACS Chem. Neurosci. 8 (2017) 2778–2790.
[119] I. Kaya, D. Brinet, W. Michno, et al., Delineating amyloid plaque associated neuronal sphingolipids in transgenic Alzheimer's disease mice (tgArcSwe) using MALDI imaging mass spectrometry, ACS Chem. Neurosci. 8 (2017) 347–355.
[120] H. Hulme, E. Fridjonsdottir, H. Gunnarsdottir, et al., Simultaneous mass spectrometry imaging of multiple neuropeptides in the brain and alterations induced by experimental parkinsonism and L-DOPA therapy, Neurobiol. Dis. 137 (2020), 104738.
[121] H. Liu, R. Chen, J. Wang, et al., 1,5-diaminonaphthalene hydrochloride assisted laser desorption/ionization mass spectrometry imaging of small

molecules in tissues following focal cerebral ischemia, Anal. Chem. 86 (2014) 10114–10121.
[122] M. Irie, Y. Fujimura, M. Yamato, et al., Integrated MALDI-MS imaging and LC-MS techniques for visualizing spatiotemporal metabolomic dynamics in a rat stroke model, Metabolomics 10 (2014) 473–483.
[123] L.S. Eberlin, I. Norton, A.L. Dill, et al., Classifying human brain tumors by lipid imaging with mass spectrometry, Cancer Res. 72 (2012) 645–654.
[124] L.S. Eberlin, I. Norton, D. Orringer, et al., Ambient mass spectrometry for the intraoperative molecular diagnosis of human brain tumors, Proc. Natl. Acad. Sci. U S A 110 (2013) 1611–1616.
[125] H.M. Brown, V. Pirro, R.G. Cooks, From DESI to the MasSpec Pen: Ambient ionization mass spectrometry for tissue analysis and intrasurgical cancer diagnosis, Clin. Chem. 64 (2018) 628–630.
[126] V. Pirro, L.S. Eberlin, P. Oliveri, et al., Interactive hyperspectral approach for exploring and interpreting DESI-MS images of cancerous and normal tissue sections, Analyst 137 (2012) 2374–2380.
[127] J.A. Losman, W.G. Kaelin Jr., What a difference a hydroxyl makes: Mutant IDH, (*R*)-2-hydroxyglutarate, and cancer, Genes Dev. 27 (2013) 836–852.
[128] L. Dang, D.W. White, S. Gross, et al., Cancer-associated IDH1 mutations produce 2-hydroxyglutarate, Nature 462 (2009) 739–744.
[129] S. Santagata, L.S. Eberlin, I. Norton, et al., Intraoperative mass spectrometry mapping of an onco-metabolite to guide brain tumor surgery, Proc. Natl. Acad. Sci. U S A 111 (2014) 11121–11126.
[130] C. Esteve, E.A. Tolner, R. Shyti, et al., Mass spectrometry imaging of amino neurotransmitters: A comparison of derivatization methods and application in mouse brain tissue, Metabolomics 12 (2016), 30.
[131] A. Kleinridders, H.A. Ferris, M.L. Reyzer, et al., Regional differences in brain glucose metabolism determined by imaging mass spectrometry, Mol. Metab. 12 (2018) 113–121.
[132] R.J. McCrimmon, C.M. Ryan, B.M. Frier, Diabetes and cognitive dysfunction, Lancet 379 (2012) 2291–2299.
[133] V. Srikanth, A.J. Sinclair, F. Hill-Briggs, et al., Type 2 diabetes and cognitive dysfunction-towards effective management of both comorbidities, Lancet Diabetes Endocrinol. 8 (2020) 535–545.
[134] D.R. Bandura, V.I. Baranov, O.I. Ornatsky, et al., Mass cytometry: Technique for real time single cell multitarget immunoassay based on inductively coupled plasma time-of-flight mass spectrometry, Anal. Chem. 81 (2009) 6813–6822.
[135] C. Böttcher, S. Schlickeiser, M.A.M. Sneeboer, et al., Human microglia regional heterogeneity and phenotypes determined by multiplexed single-cell mass cytometry, Nat. Neurosci. 22 (2019) 78–90.
[136] A.Z. Wang, J.A. Bowman-Kirigin, R. Desai, et al., Single-cell profiling of human dura and meningioma reveals cellular meningeal landscape and insights into meningioma immune response, Genome Med. 14 (2022), 49.
[137] C. Park, G. Ponath, M. Levine-Ritterman, et al., The landscape of myeloid and astrocyte phenotypes in acute multiple sclerosis lesions, Acta Neuropathol. Commun. 7 (2019), 130.
[138] V. Ramaglia, S. Sheikh-Mohamed, K. Legg, et al., Multiplexed imaging of immune cells in staged multiple sclerosis lesions by mass cytometry, eLife 8 (2019), 48051.
[139] D.W. Moon, Y.H. Park, S.Y. Lee, et al., Multiplex protein imaging with secondary ion mass spectrometry using metal oxide nanoparticle-conjugated antibodies, ACS Appl. Mater. Interfaces 12 (2020) 18056–18064.
[140] J. Cox, M. Mann, MaxQuant enables high peptide identification rates, individualized p.p.b.-range mass accuracies and proteome-wide protein quantification, Nat. Biotechnol. 26 (2008) 1367–1372.
[141] M. Holzlechner, S. Reitschmidt, S. Gruber, et al., Visualizing fungal metabolites during mycoparasitic interaction by MALDI mass spectrometry imaging, Proteomics 16 (2016) 1742–1746.
[142] H. Tsugawa, T. Cajka, T. Kind, et al., MS-DIAL: Data-independent MS/MS deconvolution for comprehensive metabolome analysis, Nat. Methods 12 (2015) 523–526.
[143] A. Andersson, J. Bergenstråhle, M. Asp, et al., Single-cell and spatial transcriptomics enables probabilistic inference of cell type topography, Commun. Biol. 3 (2020), 565.
[144] X. Qiu, D.Y. Zhu, J. Yao, et al., Spateo: Multidimensional spatiotemporal modeling of single-cell spatial transcriptomics, bioRxiv. (2022). https://doi.org/10.1101/2022.12.07.519417.
[145] M. Elosua-Bayes, P. Nieto, E. Mereu, et al., SPOTlight: Seeded NMF regression to deconvolute spatial transcriptomics spots with single-cell transcriptomes, Nucleic Acids Res. 49 (2021), e50.
[146] R. Zeira, M. Land, A. Strzalkowski, et al., Alignment and integration of spatial transcriptomics data, Nat. Methods 19 (2022) 567–575.
[147] J. Liao, J. Qian, Y. Fang, et al., *De novo* analysis of bulk RNA-seq data at spatially resolved single-cell resolution, Nat. Commun. 13 (2022), 6498.
[148] Y. Hao, S. Hao, E. Andersen-Nissen, et al., Integrated analysis of multimodal single-cell data, Cell 184 (2021) 3573–3587.e29.
[149] X. Qian, K.D. Harris, T. Hauling, et al., Probabilistic cell typing enables fine mapping of closely related cell types *in situ*, Nat. Methods 17 (2020) 101–106.
[150] D. Sun, Z. Liu, T. Li, et al., STRIDE: Accurately decomposing and integrating spatial transcriptomics using single-cell RNA sequencing, Nucleic Acids Res. 50 (2022), e42.
[151] V. Svensson, S.A. Teichmann, O. Stegle, SpatialDE: Identification of spatially variable genes, Nat. Methods 15 (2018) 343–346.
[152] S. Sun, J. Zhu, X. Zhou, Statistical analysis of spatial expression patterns for spatially resolved transcriptomic studies, Nat. Methods 17 (2020) 193–200.
[153] D. Pham, X. Tan, J. Xu, et al., stLearn: Integrating spatial location, tissue morphology and gene expression to find cell types, cell-cell interactions and spatial trajectories within undissociated tissues, bioRxiv. (2020). https://doi.org/10.1101/2020.05.31.125658.
[154] V. Kleshchevnikov, A. Shmatko, E. Dann, et al., Cell2location maps fine-grained cell types in spatial transcriptomics, Nat. Biotechnol. 40 (2022) 661–671.
[155] E.M. Holgersen, S. Gandhi, Y. Zhou, et al., Transcriptome-wide off-target effects of steric-blocking oligonucleotides, Nucleic Acid Ther. 31 (2021) 392–403.
[156] Q. Zhu, S. Shah, R. Dries, et al., Identification of spatially associated subpopulations by combining scRNAseq and sequential fluorescence *in situ* hybridization data, Nat. Biotechnol. 36 (2018) 1183–1190.
[157] R. Dries, Q. Zhu, R. Dong, et al., Giotto: A toolbox for integrative analysis and visualization of spatial expression data, Genome Biol. 22 (2021), 78.
[158] K.H. Tang, S. Li, A. Khodadadi-Jamayran, et al., Combined inhibition of SHP2 and CXCR1/2 promotes antitumor T-cell response in NSCLC, Cancer Discov. 12 (2022) 47–61.
[159] K.W. Govek, E.C. Troisi, Z. Miao, et al., Single-cell transcriptomic analysis of mIHC images via antigen mapping, Sci. Adv. 7 (2021), eabc5464.
[160] X. Shao, C. Li, H. Yang, et al., Knowledge-graph-based cell-cell communication inference for spatially resolved transcriptomic data with SpaTalk, Nat. Commun. 13 (2022), 4429.
[161] C. Wang, D. Sun, X. Huang, et al., Integrative analyses of single-cell transcriptome and regulome using MAESTRO, Genome Biol. 21 (2020), 198.
[162] H.J. Kim, Y. Lin, T.A. Geddes, et al., CiteFuse enables multi-modal analysis of CITE-seq data, Bioinformatics 36 (2020) 4137–4143.
[163] A. Gayoso, Z. Steier, R. Lopez, et al., Joint probabilistic modeling of single-cell multi-omic data with totalVI, Nat. Methods 18 (2021) 272–282.
[164] S. Jin, L. Zhang, Q. Nie, scAI: An unsupervised approach for the integrative analysis of parallel single-cell transcriptomic and epigenomic profiles, Genome Biol. 21 (2020), 25.
[165] R. Argelaguet, D. Arnol, D. Bredikhin, et al., MOFA+: A statistical framework for comprehensive integration of multi-modal single-cell data, Genome Biol. 21 (2020), 111.
[166] X. Wang, Z. Sun, Y. Zhang, et al., BRE-SC: A bayesian random effects mixture model for joint clustering single cell multi-omics data, Nucleic Acids Res. 48 (2020) 5814–5824.
[167] W. Liu, X. Liao, Z. Luo, et al., Probabilistic embedding, clustering, and alignment for integrating spatial transcriptomics data with PRECAST, Nat. Commun. 14 (2023), 296.
[168] K. Cao, X. Bai, Y. Hong, et al., Unsupervised topological alignment for single-cell multi-omics integration, Bioinformatics 36 (2020) i48–i56.
[169] J.D. Welch, V. Kozareva, A. Ferreira, et al., Single-cell multi-omic integration compares and contrasts features of brain cell identity, Cell 177 (2019) 1873–1887.e17.
[170] M. Stevens, A. Nanou, L. Terstappen, et al., StarDist image segmentation improves circulating tumor cell detection, Cancers (Basel) 14 (2022), 2916.
[171] S. Mandal, V. Uhlmann, SplineDist: Automated cell segmentation with spline curves, bioRxiv. (2021). https://doi.org/10.1101/2020.10.27.357640.
[172] C. Stringer, T. Wang, M. Michaelos, et al., Cellpose: A generalist algorithm for cellular segmentation, Nat. Methods 18 (2021) 100–106.
[173] C.W. Grant, E.F. Barreto, R. Kumar, et al., Multi-omics characterization of early- and adult-onset major depressive disorder, J. Pers. Med. 12 (2022), 412.
[174] S. Vickovic, B. Lötstedt, J. Klughammer, et al., SM-Omics is an automated platform for high-throughput spatial multi-omics, Nat. Commun. 13 (2022), 795.
[175] V. Kumar, K. Ramnarayanan, R. Sundar, et al., Single-cell atlas of lineage states, tumor microenvironment, and subtype-specific expression programs in gastric cancer, Cancer Discov. 12 (2022) 670–691.
[176] S. Prokop, K.R. Miller, S.R. Labra, et al., Impact of TREM2 risk variants on brain region-specific immune activation and plaque microenvironment in Alzheimer's disease patient brain samples, Acta Neuropathol. 138 (2019) 613–630.
[177] M. Kaufmann, A.L. Schaupp, R. Sun, et al., Identification of early neurodegenerative pathways in progressive multiple sclerosis, Nat. Neurosci. 25 (2022) 944–955.
[178] V.M. Ravi, P. Will, J. Kueckelhaus, et al., Spatially resolved multi-omics deciphers bidirectional tumor-host interdependence in glioblastoma, Cancer Cell 40 (2022) 639–655.e13.
[179] A.K. Ottens, The methodology of neuroproteomics, Methods Mol. Biol. 566 (2009) 1–21.
[180] H. Haas, P. Panula, The role of histamine and the tuberomamillary nucleus in the nervous system, Nat. Rev. Neurosci. 4 (2003) 121–130.
[181] G.M. Shepherd, M. Raastad, Axonal varicosity distributions along parallel fibers: A new angle on a cerebellar circuit, Cerebellum 2 (2003) 110–113.
[182] N.N. Foster, J. Barry, L. Korobkova, et al., The mouse cortico-basal ganglia-thalamic network, Nature 598 (2021) 188–194.

[183] BRAIN Initiative Cell Census Network (BICCN), A multimodal cell census and atlas of the mammalian primary motor cortex, Nature 598 (2021) 86–102.
[184] H. Peng, P. Xie, L. Liu, et al., Morphological diversity of single neurons in molecularly defined cell types, Nature 598 (2021) 174–181.
[185] W. Yang, R. Yuste, *In vivo* imaging of neural activity, Nat. Methods 14 (2017) 349–359.
[186] C. Grienberger, A. Konnerth, Imaging calcium in neurons, Neuron 73 (2012) 862–885.
[187] W. Pei, T.B. Feyerabend, J. Rössler, et al., Polylox barcoding reveals haematopoietic stem cell fates realized *in vivo*, Nature 548 (2017) 456–460.
[188] X. Qian, H. Song, G.-L. Ming, Brain organoids: Advances, applications and challenges, Development 146 (2019), dev166074.
[189] K. Watanabe, D. Kamiya, A. Nishiyama, et al., Directed differentiation of telencephalic precursors from embryonic stem cells, Nat. Neurosci. 8 (2005) 288–296.
[190] K. Watanabe, M. Ueno, D. Kamiya, et al., A ROCK inhibitor permits survival of dissociated human embryonic stem cells, Nat. Biotechnol. 25 (2007) 681–686.
[191] B. Bakker, R.D.W. Vaes, M.R. Aberle, et al., Preparing ductal epithelial organoids for high-spatial-resolution molecular profiling using mass spectrometry imaging, Nat. Protoc. 17 (2022) 962–979.
[192] M.L. Spruill, M. Maletic-Savatic, H. Martin, et al., Spatial analysis of drug absorption, distribution, metabolism, and toxicology using mass spectrometry imaging, Biochem. Pharmacol. 201 (2022), 115080.
[193] M.K. Passarelli, A. Pirkl, R. Moellers, et al., The 3D OrbiSIMS-label-free metabolic imaging with subcellular lateral resolution and high mass-resolving power, Nat. Methods 14 (2017) 1175–1183.
[194] M.T. Proetto, C.R. Anderton, D. Hu, et al., Cellular delivery of nanoparticles revealed with combined optical and isotopic nanoscopy, ACS Nano 10 (2016) 4046–4054.
[195] V.J. Orphan, C.H. House, K.U. Hinrichs, et al., Methane-consuming archaea revealed by directly coupled isotopic and phylogenetic analysis, Science 293 (2001) 484–487.